

NATIONAL BUREAU OF STANDARDS REPORT

6255

PROPERTY OF
SOUTHWEST RESEARCH INSTITUTE LIBRARY
SAN ANTONIO, TEXAS

ELASTIC SCATTERING OF PHOTONS

FINAL REPORT

1. January 1959

by

E. G. Fuller and Evans Hayward
High Energy Radiation Section
Atomic and Radiation Physics Division

to

Nuclear Physics Division
Air Force Office of Scientific Research, ARDC
Washington 25, D. C.

CONTRACT NO. 680-58-16

FILE NO. 3-1-8



U. S. DEPARTMENT OF COMMERCE
NATIONAL BUREAU OF STANDARDS

THE NATIONAL BUREAU OF STANDARDS

Functions and Activities

The functions of the National Bureau of Standards are set forth in the Act of Congress, March 3, 1901, as amended by Congress in Public Law 619, 1950. These include the development and maintenance of the national standards of measurement and the provision of means and methods for making measurements consistent with these standards; the determination of physical constants and properties of materials; the development of methods and instruments for testing materials, devices, and structures; advisory services to Government Agencies on scientific and technical problems; invention and development of devices to serve special needs of the Government; and the development of standard practices, codes, and specifications. The work includes basic and applied research, development, engineering, instrumentation, testing, evaluation, calibration services, and various consultation and information services. A major portion of the Bureau's work is performed for other Government Agencies, particularly the Department of Defense and the Atomic Energy Commission. The scope of activities is suggested by the listing of divisions and sections on the inside of the back cover.

Reports and Publications

The results of the Bureau's work take the form of either actual equipment and devices or published papers and reports. Reports are issued to the sponsoring agency of a particular project or program. Published papers appear either in the Bureau's own series of publications or in the journals of professional and scientific societies. The Bureau itself publishes three monthly periodicals, available from the Government Printing Office: The Journal of Research, which presents complete papers reporting technical investigations; the Technical News Bulletin, which presents summary and preliminary reports on work in progress; and Basic Radio Propagation Predictions, which provides data for determining the best frequencies to use for radio communications throughout the world. There are also five series of nonperiodical publications: The Applied Mathematics Series, Circulars, Handbooks, Building Materials and Structures Reports, and Miscellaneous Publications.

Information on the Bureau's publications can be found in NBS Circular 460, Publications of the National Bureau of Standards (\$1.25) and its Supplement (\$0.75), available from the Superintendent of Documents, Government Printing Office, Washington 25, D. C.

Inquiries regarding the Bureau's reports should be addressed to the Office of Technical Information, National Bureau of Standards, Washington 25, D. C.

NATIONAL BUREAU OF STANDARDS REPORT

NBS PROJECT

NBS REPORT

0411-11-3154

1 January 1959

6255

ELASTIC SCATTERING OF PHOTONS

by

E. G. Fuller and Evans Hayward
High Energy Radiation Section
Atomic and Radiation Physics Division

to

Nuclear Physics Division
Air Force Office of Scientific Research, ARDC
Washington 25, D. C.

CONTRACT NO. 680-58-16

FILE NO. 3-1-8

IMPORTANT NOTICE

NATIONAL BUREAU OF STANDARDS
Intended for use within the Government.
This report is not to be distributed
to additional evaluation and review
listing of this Report, either in whole
the Office of the Director, National
however, by the Government agency
to reproduce additional copies for

Approved for public release by the
Director of the National Institute of
Standards and Technology (NIST) on
October 9, 2015.

When accounting documents
are published it is subjected
reproduction, or open-literature
is obtained in writing from
such permission is not needed,
prepared if that agency wishes



U. S. DEPARTMENT OF COMMERCE

NATIONAL BUREAU OF STANDARDS

Summary of Elastic Scattering Cross Section
Measurements

In 1952 Stearns^{1/} showed that it was possible to measure the elastic
^{1/}M.B. Stearns, Phys. Rev. 87, 706 (1952).

scattering of 17.6 Mev photons by using a biased NaI(Tl) spectrometer.
This technique has been applied^{2/} using betatron X-rays to measure the
^{2/}E. G. Fuller and E. Hayward, Phys. Rev. 101, 692 (1956). (Reprint attached).
elastic scattering cross sections for a number of elements in the energy
range 4-40 Mev. (An evaluation of this technique for measuring elastic
scattering cross sections is given at the end of this summary). In this
survey experiment the elastic scattering cross sections were found, in
general, to consist of two maxima. The cross section rises to a maximum
and then falls sharply at the threshold for particle emission; it then rises
once more and goes through a broad resonance that resembles the neutron
emission cross section except that it is a factor of about a hundred smaller
in magnitude.

The scattering in these two energy regions is produced by two different
kinds of nuclear properties. The lower energy maximum results from the
fluorescence of a number of discrete energy levels, unresolved by the NaI(Tl)
spectrometer. The size of the scattering cross section here is a measure
of the number and widths of the levels, making ground-state transitions in
the particular nucleus under consideration. On the other hand, the scattering
observed in the giant resonance region results from oscillations of the
whole nucleus and is associated with the electric dipole absorption that
usually results in the emission of neutrons or protons. The size of the
latter scattering cross sections is, therefore, a smooth function of Z.

The measurements were performed at a backward angle in order to avoid backgrounds. This had the additional advantage that nonnuclear coherent scattering, such as Rayleigh and Delbruck scattering, which are both peaked very strongly forward, went undetected. The measured cross sections then are produced by nuclear Thomson scattering and the scattering associated with the elastic deformation of the nuclear charge distribution.

The total scattering cross sections have been obtained from those measured at 120° on the assumption that the angular distribution was given by $(1 + \cos^2 \theta)$, i.e. that the scattering is electric dipole and results from a scalar polarizability of the nucleus. Since the forward scattering cross section is related to the total absorption cross section by a dispersion relation, it has been possible to compare the measured elastic scattering cross sections in the giant resonance region with the nuclear absorption cross sections obtained in other experiments. Crude comparisons made in reference 2, using data available in 1955, showed consistency between the elastic scattering and total absorption cross sections for elements heavier than copper. More recently a code has been written for the IBM 704 computer which facilitates these computations enormously. The neutron yield cross sections, recently obtained in this laboratory, have been used to predict in detail the elastic scattering cross sections for Sn, I, Pb, and Au. These are also in good agreement with the cross sections reported in reference 2. (See Figs. 1 to 4).

Very recently the elastic scattering cross section for the deformed nucleus Ta^{181} has been measured for comparison with the neutron yield cross section obtained by Fuller and Weiss^{3/}. They have shown that the

^{3/} E. G. Fuller and M. Weiss, Phys. Rev. 112, 554 and 560 (1958).

photon absorption cross section has two maxima associated with two modes of oscillation of the nuclear charge. In order to predict satisfactorily the observed scattering cross section from the neutron yield cross section it was necessary to assume that the nuclear polarizability is a tensor.^{4/}

^{4/}
E. G Fuller and E. Hayward, Phys. Rev. Letters 1, 465(1958).

The scattering cross section then does not have a simple dipole angular distribution but is given by $d\sigma(\theta)/d\Omega = A(1 + K(E) \cos^2\theta)$. Fig. 5 gives $K(E)$ as a function of energy. An experimental measurement of these distributions would be difficult but very desirable.

The agreement between the scattering and absorption cross sections for the light nuclei is not so satisfactory. The sums of the (γ, n) and (γ, p) cross sections are not great enough to account for the measured elastic scattering cross sections especially at energies above 20 Mev. As an example, detailed comparisons of the scattering and absorption cross sections for Al were made in reference 2. There have recently been two careful measurements on aluminum. One^{5/} obtained the total absorption

^{5/}
J. M. Wyckoff and H. W. Koch, private communication.
cross section directly, and the other^{6/} attempted to determine all the

^{6/}
Fererro et al, private communication.
partial cross sections of importance. Both are in disagreement with the elastic scattering cross section as it has been interpreted. This discrepancy may result from the assumptions made concerning the angular distribution of the elastically scattered photons used to obtain the forward scattering cross section. The distribution corresponding to electric dipole transitions was used. If the absorption at the higher energies is the result of another mode an angular distribution of the

scattering peaked in the backward direction could result. This would result in the high total cross section already reported^{2/}. Except for the fact that the measured nuclear absorption cross section does not exhaust the dipole sum, this offers a satisfactory explanation of the discrepancy. Measurements of the angular distributions of the scattered photons are certainly indicated.

In the energy region below the particle threshold, where the elastic scattering cross section frequently shows a maximum, the nuclear energy levels are narrow compared to their spacing. A measure of the peak absorption cross section in these levels can be obtained from a self-absorption experiment, if the peak absorption cross section is at least half the electronic absorption cross section. The procedure is to measure the attenuation when an absorber of the target material is placed in the incident bremsstrahlung beam. The absorber removes from the beam photons otherwise destined to excite levels in the target.

The usual situation is one in which there are a large, unknown number of unresolved levels being excited. The results obtained therefore represent some kind of average properties for the levels involved. A single isolated level can have a peak absorption cross section as high as $6\pi\lambda^2$ (more than 100 barns at 7 Mev). This level can be broadened and the peak cross section correspondingly depressed either by inelastic scattering or by thermal doppler broadening. If the broadening results from inelastic scattering, a real nuclear property, the self-absorption experiment yields the ground-state branching ratio, Γ_{gs}/Γ , for the level. If on the other hand the level is completely doppler-broadened, the ground-state width in units of the doppler width, Γ_{gs}/δ , is obtained. In principle, the observed attenuation

can be changed by changing the doppler width, i.e. the temperature of the target and absorber. Real levels are almost always broadened both by inelastic scattering and thermal effects so that the analysis is considerably more complicated. The 15.1 Mev level in C^{12} is the only isolated level found so far that is amenable to this type of investigation. This level is broadened both by inelastic scattering and thermal doppler broadening. The level parameters were therefore determined^{7/} to be those^{7/} E. Hayward and E. G. Fuller, Phys. Rev. 106, 991 (1957). (Reprint attached) most consistent with the measured integral scattering cross section and the self-absorption data.

Self-absorption has been observed for photon energies just below the particle thresholds of Mg, Al, Ni, Pb, radio Pb and Bi. This effect was sought but not found in the scattering by Mn, Cu and Sn. The observed effects produced by the many levels in the energy band under consideration, are not large and correspond to peak absorption cross sections of the same order as the electronic absorption. A recent series of measurement using targets of lead, radiopb, and bismuth included (1) a detailed determination of the elastic scattering cross section in the energy range 4-10 Mev, (2) attenuation measurements with absorbers of the same materials at room and liquid nitrogen temperatures, and (3) attenuation measurements using absorbers enriched in Pb^{208} and Pb^{209} .

These data have been analyzed to give the average properties of the levels just below the (γ, n) thresholds for these nuclei. The results were presented at the 1958 Paris Conference on Nuclear Physics. (See attached Copy)

In conclusion the following problems should be further investigated:

A. Detailed elastic scattering cross section measurements in the

giant resonance energy region with medium and heavy nuclei. Particular attention should be paid to those nuclei having large nuclear deformations.

B. Angular distribution measurements as a function of photon energy for a deformed nucleus such as Ta.

C. Careful scattering cross section measurements, both energy and angular dependence, for light nuclei. This should lead to information regarding the apparent lack of integrated absorption cross section for the nuclei.

D. Detailed studies of the self absorption effect that has been seen in Mg, Al, and Ni. This would consist of a series of experiments such as those recently completed with the lead isotopes and bismuth.

E. Systematic survey for additional self-absorption effects particularly in the lighter nuclei. This technique is one of the few available which leads to information regarding the levels just below the particle thresholds in nuclei. Particle cross section measurements usually only give information about the levels at excitations just above these thresholds.

Evaluation of Elastic Scattering Measurements

In the analysis of the elastic scattering experiment it has always been assumed that the pulse height scale was equivalent to a photon energy scale near the end of the spectrum. The crudeness of most of the measurements that have been made probably justifies this assumption. When, however, measurements were made in which the statistical uncertainties in the data were reduced to the order of 10 percent it was decided to attempt to make an estimate of what the effects of the spectral shape of the photons incident on the NaI crystal and the spectrometer response function would be on the

interpretation of the scattering cross section as normally measured.

The procedure which has evolved in measuring these cross sections has been the following: The NaI crystal is first placed in the bremsstrahlung beam and the pulse height distribution is obtained with a multi-channel analyzer for the hardened bremsstrahlung spectrum. The end point of this spectrum is obtained by making a linear extrapolation of the top 15 to 20 percent of the spectrum to zero. The scattering measurements are then made using as the "end point channel" a channel whose lower and upper bounds correspond to .85 and .95 respectively of this end point found by extrapolating the bremsstrahlung pulse height spectrum. The measured cross sections have then been plotted as an average cross section over a 10 percent energy bin centered at an energy of 0.9 times the maximum energy in the bremsstrahlung spectrum.

In terms of the actual scattering cross section $\sigma(E)$, the average cross section obtained in the scattering experiment is defined by:

$$\langle \sigma \rangle = \frac{Y_{sc}}{Y_{EP}} = \frac{\int_{.85 h_0}^{.95 h_0} dh \int_0^{E_0} dE \sigma(E) N(E, E_0) R(h, E)}{\int_{.85 h_0}^{.95 h_0} dh \int_0^{E_0} dE N(E, E_0) R(h, E)}$$

where $N(E, E_0) dE$ is the bremsstrahlung spectrum per unit monitor reading (number of photons at an energy E for a spectrum extending to E_0) and $R(h, E) dh$ is the response function for the NaI spectrometer (number of pulses produced at a pulse height h by a photon of energy E incident on the front of the crystal). This average cross section has been calculated making various assumptions about the shape of $\sigma(E)$ and the response function R . The average cross section obtained in this way has then been compared with $\sigma(E)$ to find at what energy $\langle \sigma \rangle$ should be plotted.

The shape of the response function $R(h, E)$ is rather well known for the geometry and crystal used for most of the scattering measurements as a result of the work done on the scattering by the 15.11 Mev level in C^{12} . This pulse height distribution is given in Fig. 6. The quantity which is not known is the pulse height on the distribution that should be assigned to the center of the Gaussian distribution that would be produced if the crystal absorbed all of the photon energy. It is known that this pulse height is somewhere on the high energy edge of the distribution. The calculations which will be described below were made for two assignments which are thought to be extreme limits. These corresponded to saying that the Gaussian was centered at 18 and 19 mv on the pulse height scale given in Fig. 6. The results obtained were the same in both cases so that in the following only examples calculated with the 18 mv assignment will be given.

The average cross section $\langle \sigma \rangle$ was calculated assuming (a) that the true cross section was a linearly increasing function of the energy and (b) that this cross section was a linearly decreasing function of energy. The slopes chosen were such that across a ten per cent energy interval near the end of the bremsstrahlung spectrum the cross section changed by a

factor of two. This corresponds to the sort of slopes that have been observed in the scattering work. Fig. 7 gives the photon spectrum obtained from the Schiff integrated over angle intensity spectrum and the two assumed scattering cross section shapes.

The first step was to calculate the pulse height distribution produced when the bremsstrahlung spectrum was incident on the crystal. The upper energy end of this distribution was then plotted and a linear extrapolation was made to find the end point h_0 of the spectrum as is done in the scattering experiment. This is shown in Fig. 8 for the 18 mv assignment for the center of the Gaussian. The end point channel was then taken from $.85 h_0$ to $.95 h_0$ and the quantities $Y_{E.P.}$ and Y_S were calculated. Fig. 8 gives these functions differential in photon energy, for an end point run and for a scattering runs with increasing and decreasing cross sections. These curves give the relative number of counts produced in the pulse height channel defined by the above criteria for the three different assumed photon spectral shapes incident on the crystal. Table I gives the fraction of the total number of pulses in the end point channel which are produced by photons having energies greater than $.85 E_0$, $.90 E_0$ and $.95 E_0$. These figures and the curves given in Fig. 9 then indicate just how "elastic" the elastic scattering cross section measurements are.

Table 1.

Fraction produced by	$E > .85 E_0$	$E > .90 E_0$	$E > .95 E_0$
Increasing cross section	.98	.83	.39
End Point (Flat cross section)	.94	.71	.28
Decreasing cross section	.89	.58	.17

Using the areas under the curves given in Fig. 8 the average cross

sections (Eq. 1) $\langle \sigma \rangle$ were calculated for the two assumed shapes of $\sigma(E)$. In both cases these average cross sections corresponded to the value of the cross section, $\sigma(E)$, at $E = .93 E_0$. The differential curve of Y_{EP} given in Fig. 8 indicates that for a flat cross section the data should be plotted at an energy corresponding to about $.94 E_0$. These calculations when carried out for the 19 mv assignment of the center of the Gaussian (Fig. 6) gave the same conclusions as reached here. This is the result of the way in which the end point channel is chosen.

In the above calculations nothing is said about the sensitivity of the results obtained in the scattering experiment to the particular channel chosen for the end point channel. The following tables give an indication of how serious a problem this is. Table II gives the average cross section calculated using a channel width of $.02 E_0$ as a function of the position of this channel in the spectrum. Table III gives the average cross section calculated for a bin width of $0.10 E_0$ for three different end point extrapolations. Both of these tables indicate that, providing the end point is chosen high enough in the pulse height spectrum the scattering cross sections are independent of choice of end point to within something of the order of 5-10 percent. In order to make measurements with a higher precision than this, it would be necessary to work at the extreme end of the pulse height spectrum where counting rates would be extremely low and where the results would be strongly influenced by pile-up effects.

Conclusions

A. In regions where the scattering cross section is flat with photon energy the experimental points should be plotted at $.94 E_0$, where E_0 is

the maximum energy in the bremsstrahlung spectrum. Where the cross section is either rising or falling rapidly the points should be plotted at $.93 E_0$. In all cases the measured cross sections are averages over a photon bin approximately $0.1 E_0$ wide. (The procedure which has been followed has been to plot the data at $0.9 E_0$ and indicate it being an average over a region of about $0.1 E_0$).

B. No matter what the shape of the scattering cross section inelastic scattering can only be measured to levels within $0.15 E_0$ of the ground state. For a sharply rising cross section only levels within $0.10 E_0$ must be considered.

C. These conclusions are independent of the assignment made for the center of the Gaussian in the response function for the Na J(Tl) spectrometer.

D. The scattering cross sections calculated in this experiment are sensitive to the choice of end point channel. These errors will be of the order of 5-10 percent providing the end point channel is chosen high enough in the pulse height spectrum.

Table II (2% Channel)

Pulse Ht.	(σ rising)	(σ falling)
.85	.79	1.73
.87	.93	1.60
.89	1.04	1.46
.91	1.16	1.34
.93	1.27	1.24
.95	1.37	1.13
.97	1.46	1.05
.99	1.56	1.00
1.01	1.57	.92
1.03	1.62	.88
1.05	1.67	.85
1.07	1.75	.80
1.09	1.79	.74
1.11	1.86	.65
1.13	2.00	.60

Table III (10% Channel)

End Point	(σ rising)	(σ falling)
1.00	1.01	1.50
1.025	1.20	1.30
1.05	1.26	1.26
1.075	1.38	1.13

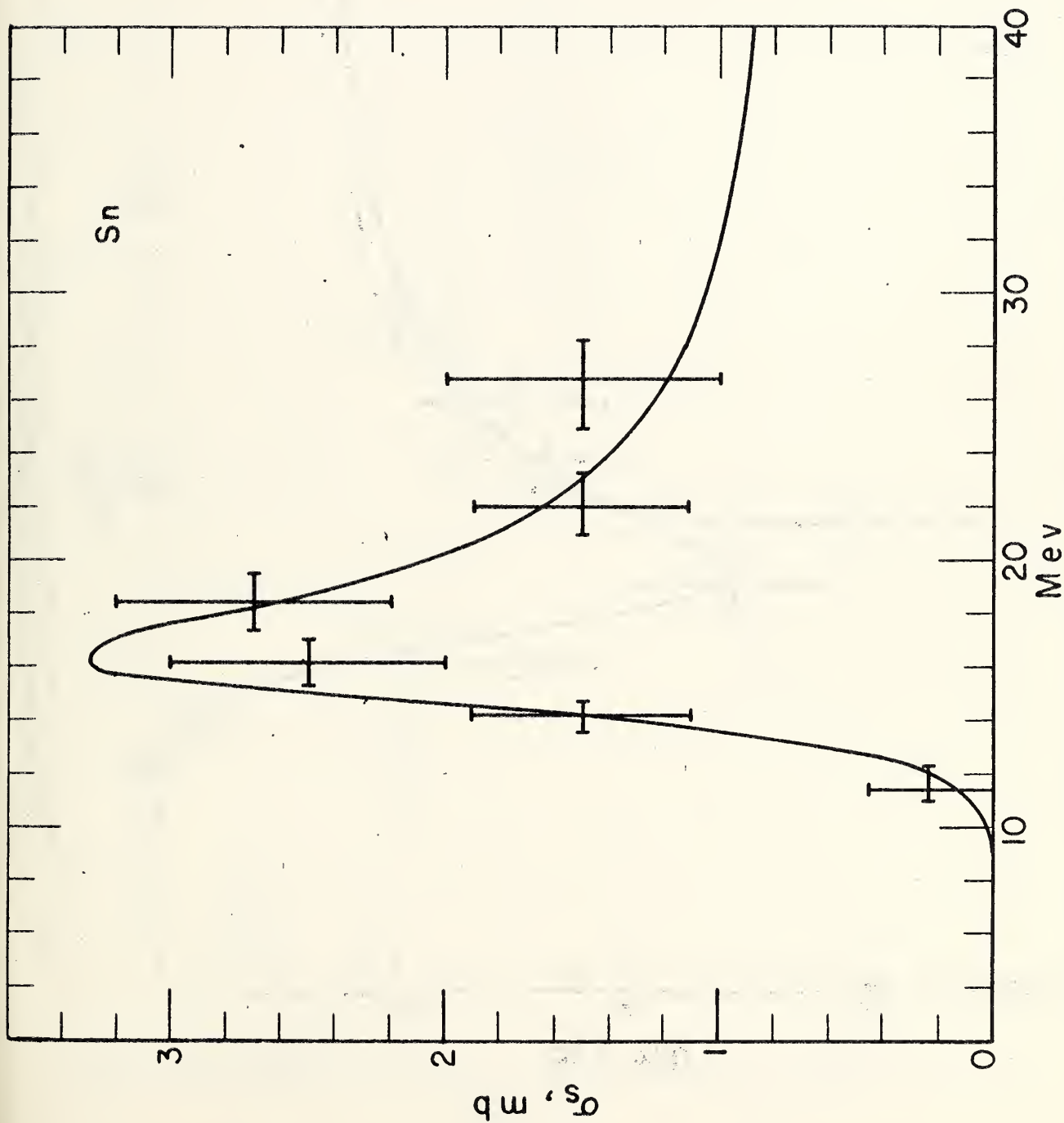


Fig. 1. The elastic scattering cross section for tin. The solid curve has been calculated from the measured neutron yield cross section.

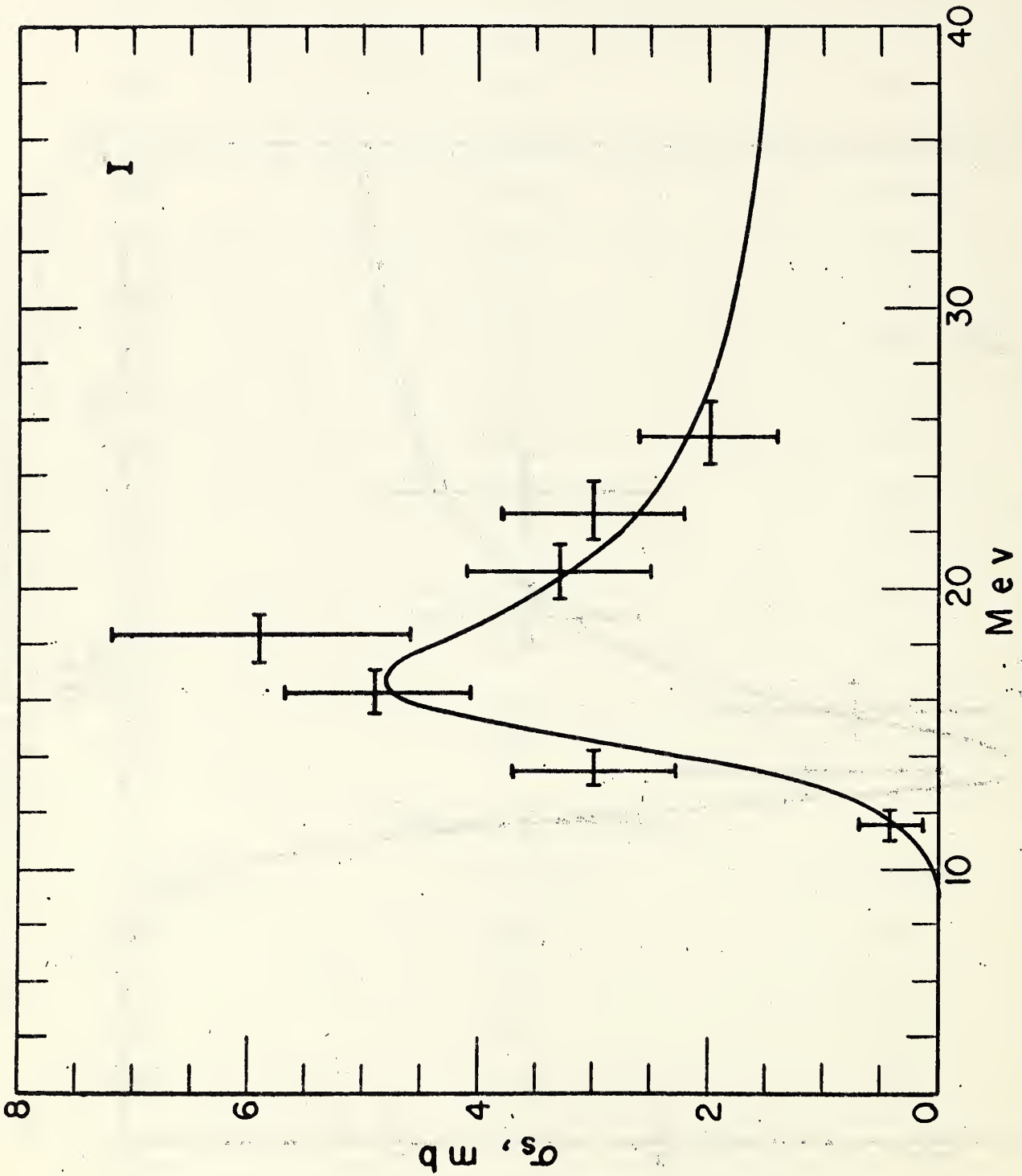


Fig. 2. The elastic scattering cross section for iodine. The solid curve has been calculated from the measured neutron yield cross section.

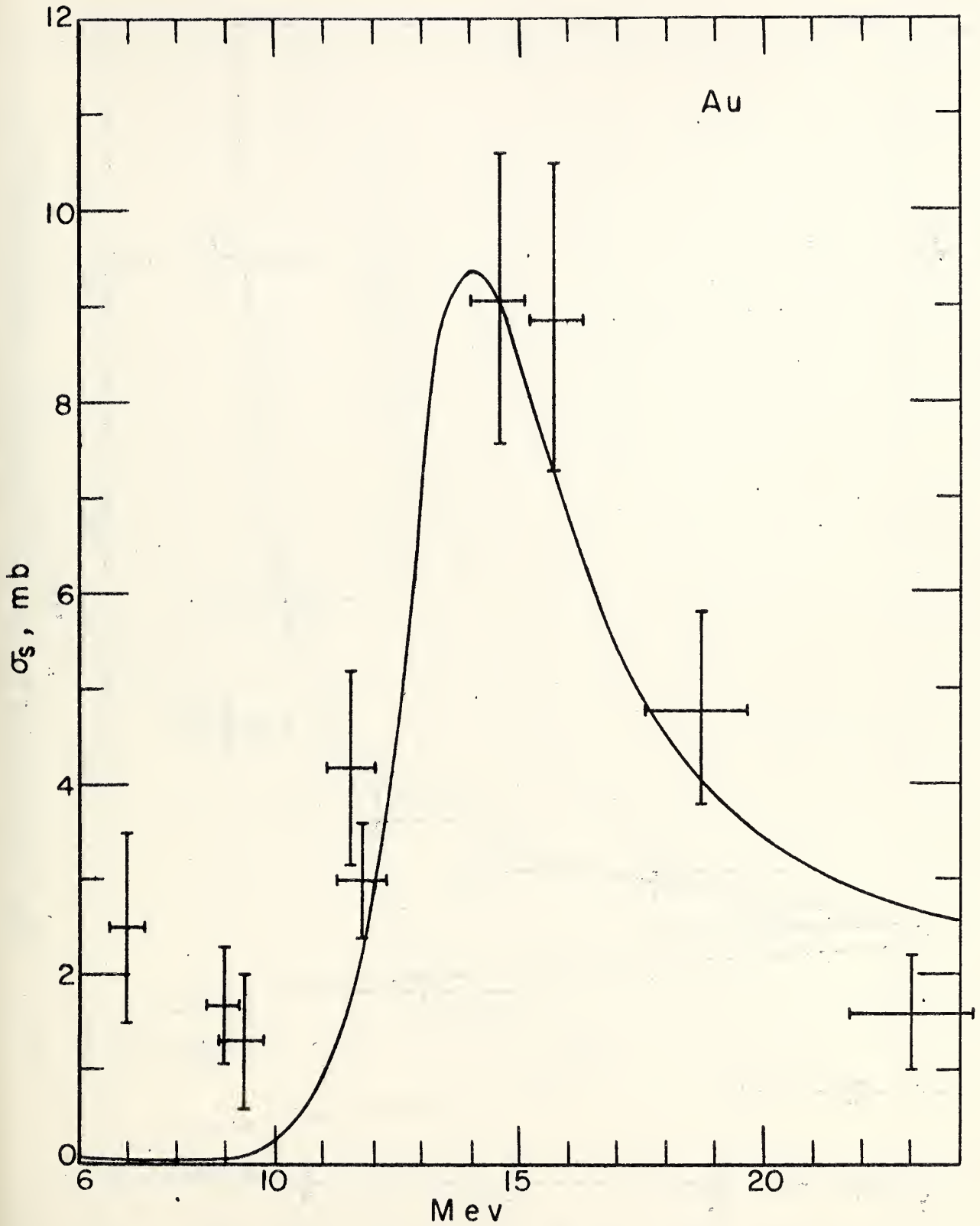


Fig. 3. The elastic scattering cross section for gold. The solid curve has been calculated from the measured neutron yield cross section.

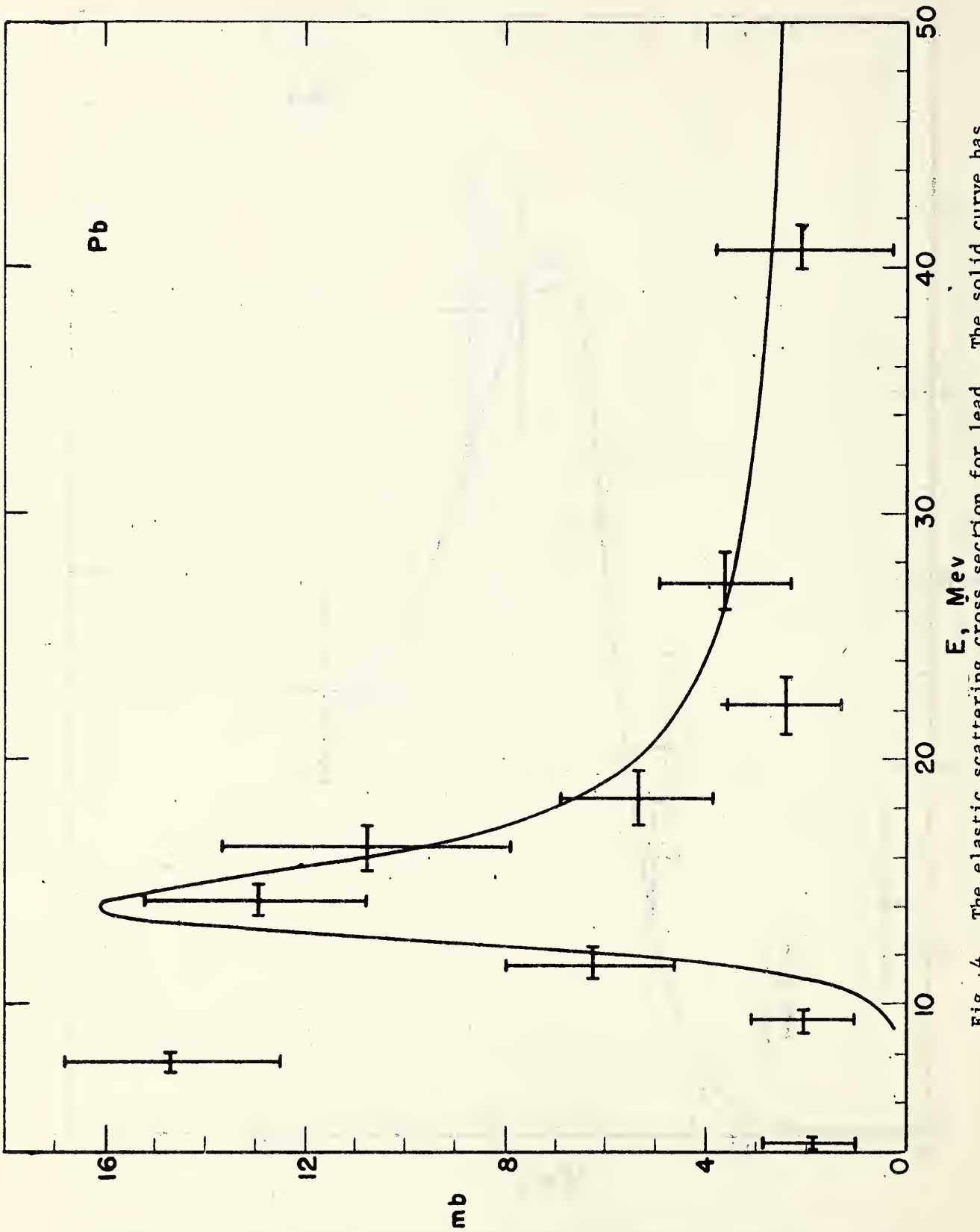


Fig. 4. The elastic scattering cross section for lead. The solid curve has been calculated from the measured neutron yield cross section.

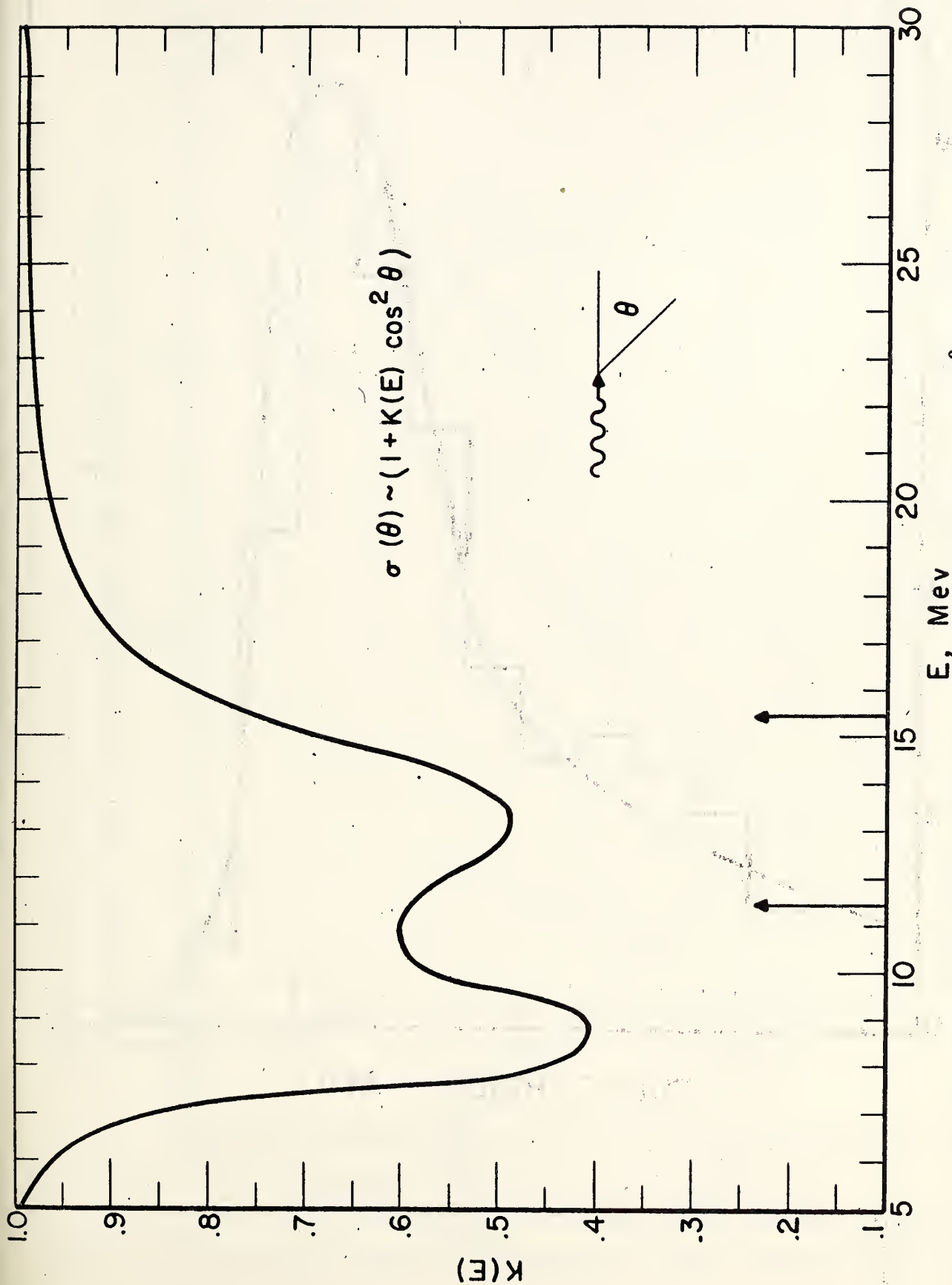


Fig. 5. $K(E)$ as a function of energy where $d\sigma/d\Omega = A(1 + K(E) \cos^2 \theta)$ is the angular distribution of the photons scattered by Ta. The vertical arrows at the bottom of the figure indicate the positions of the two resonance energies.

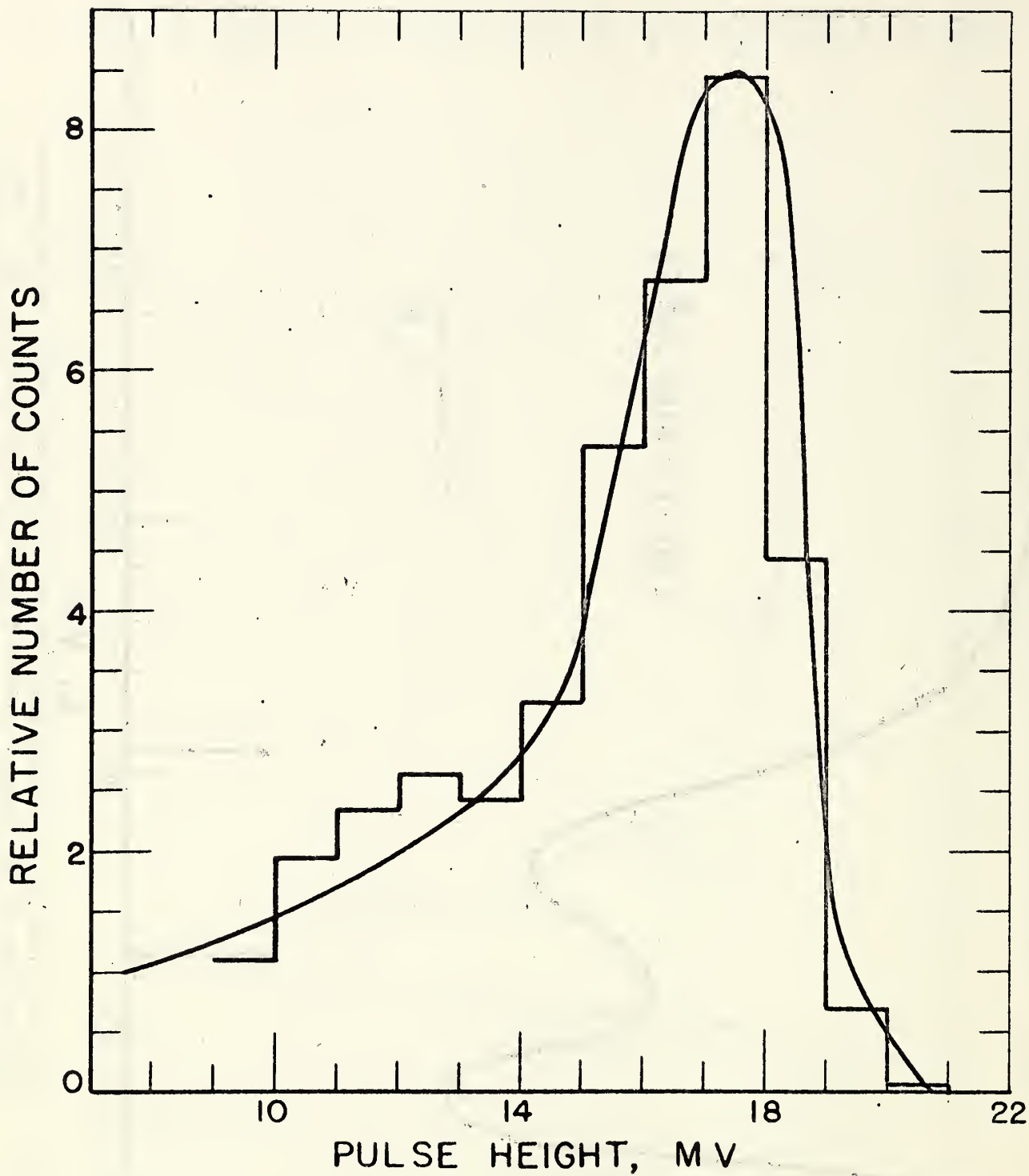


Fig. 6. The pulse height distribution produced by 15.1 Mev photons.

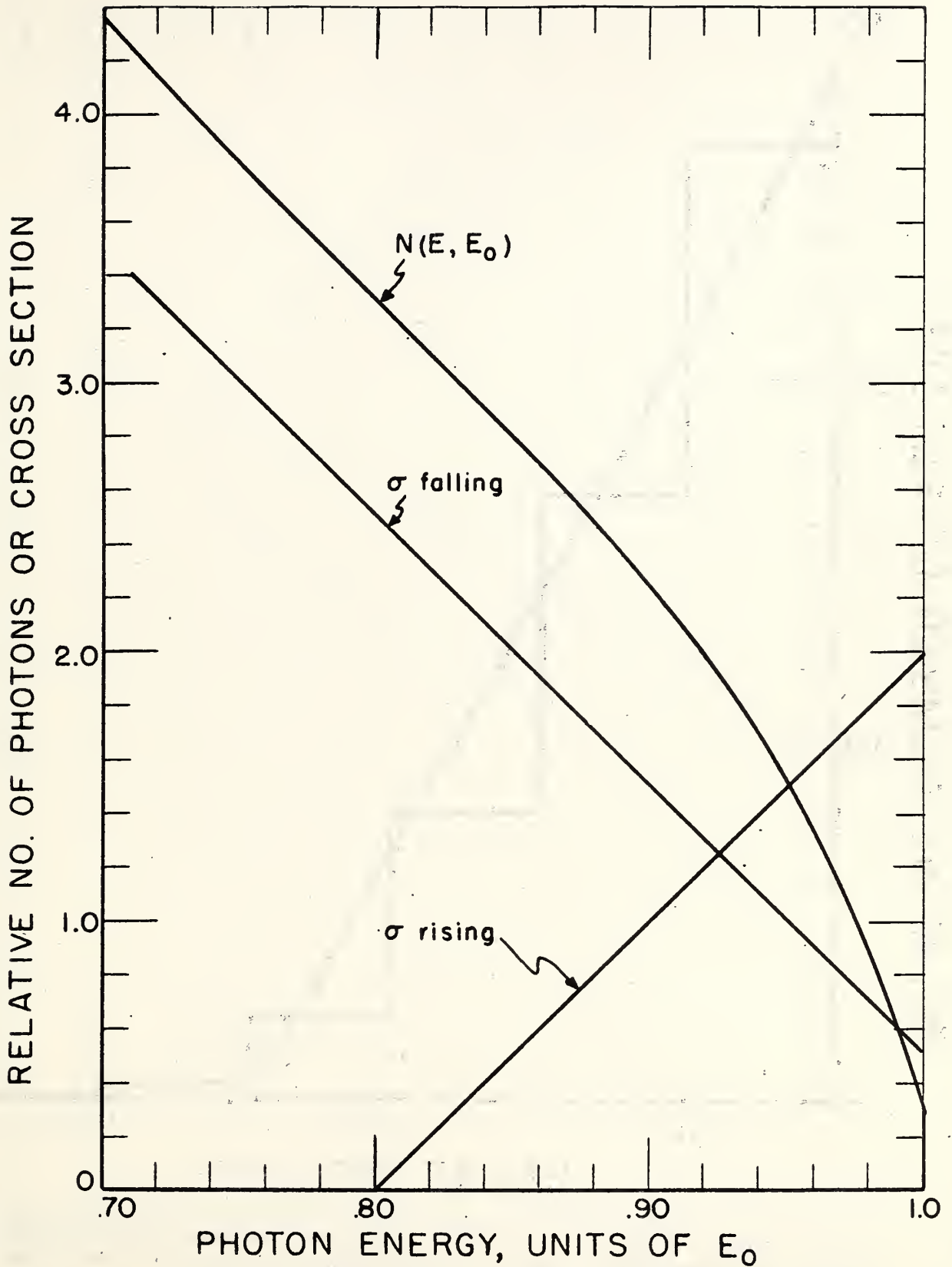


Fig. 7. The spectrum of photons obtained from the Schiff integrated over angle intensity spectrum and the two assumed scattering cross section shapes.

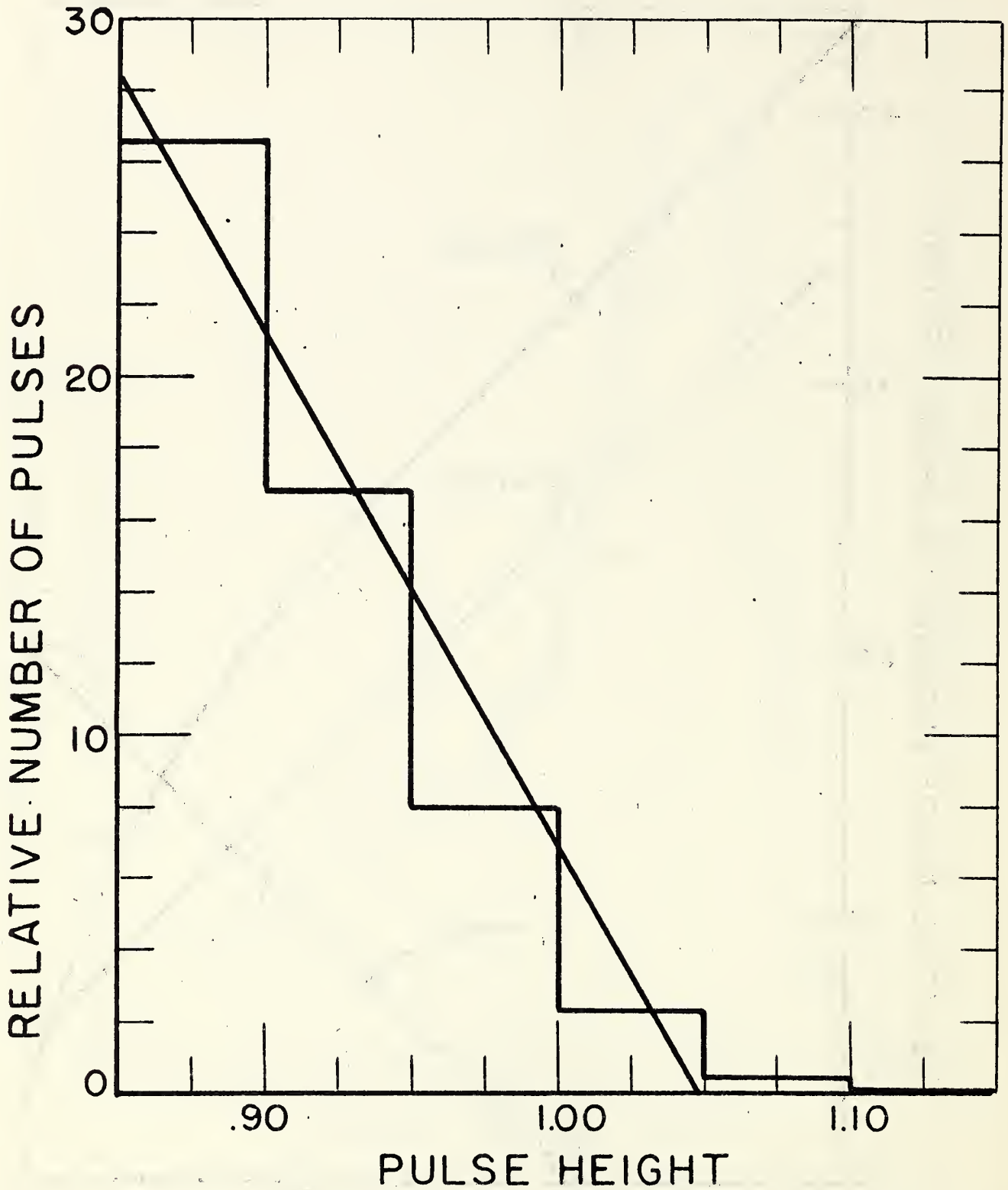


Fig. 8. The pulse height distribution calculated for the case when the bremsstrahlung is incident on the NaI(Tl) crystal. The extrapolation used to obtain the end point of the spectrum is shown.

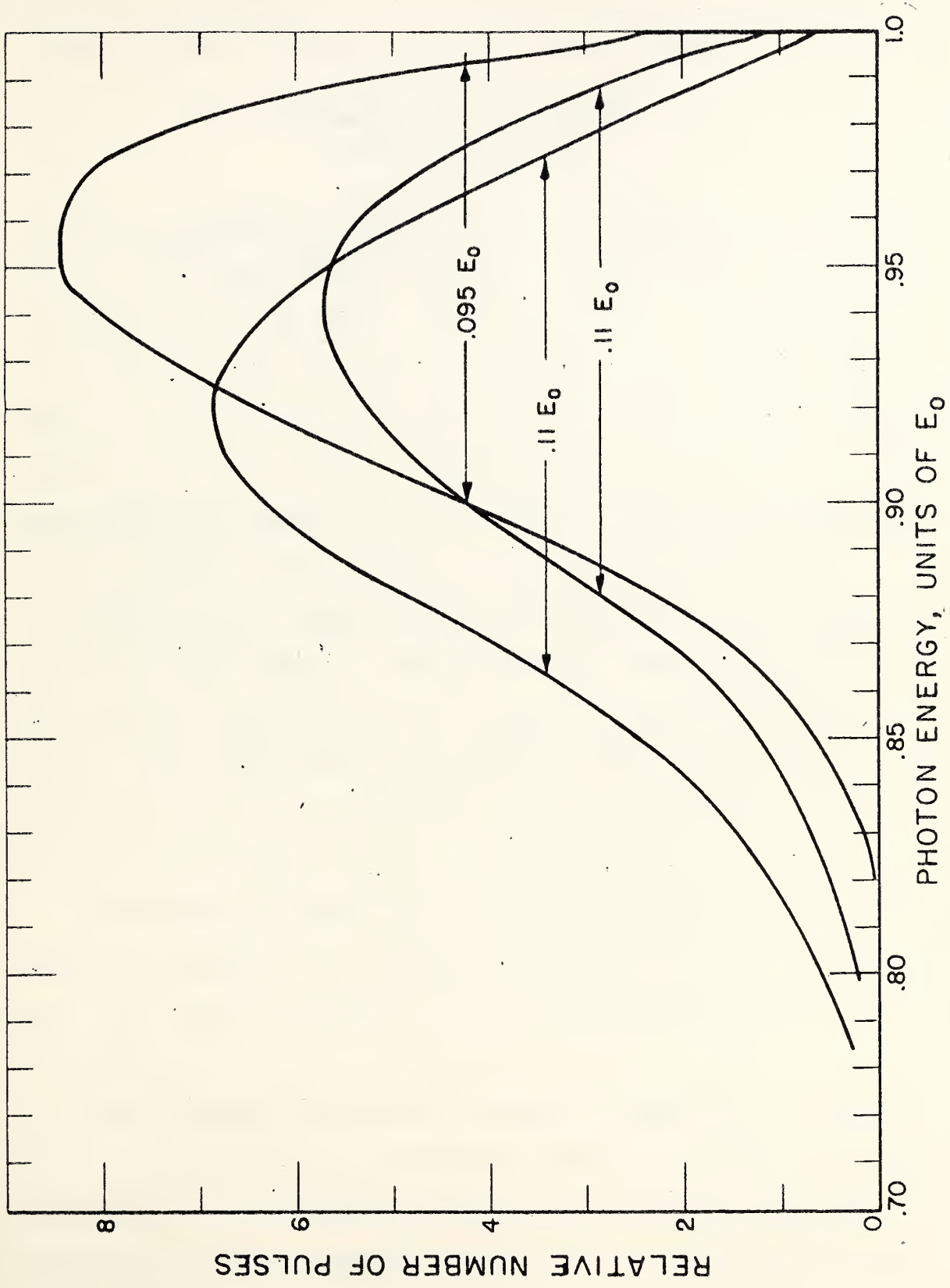
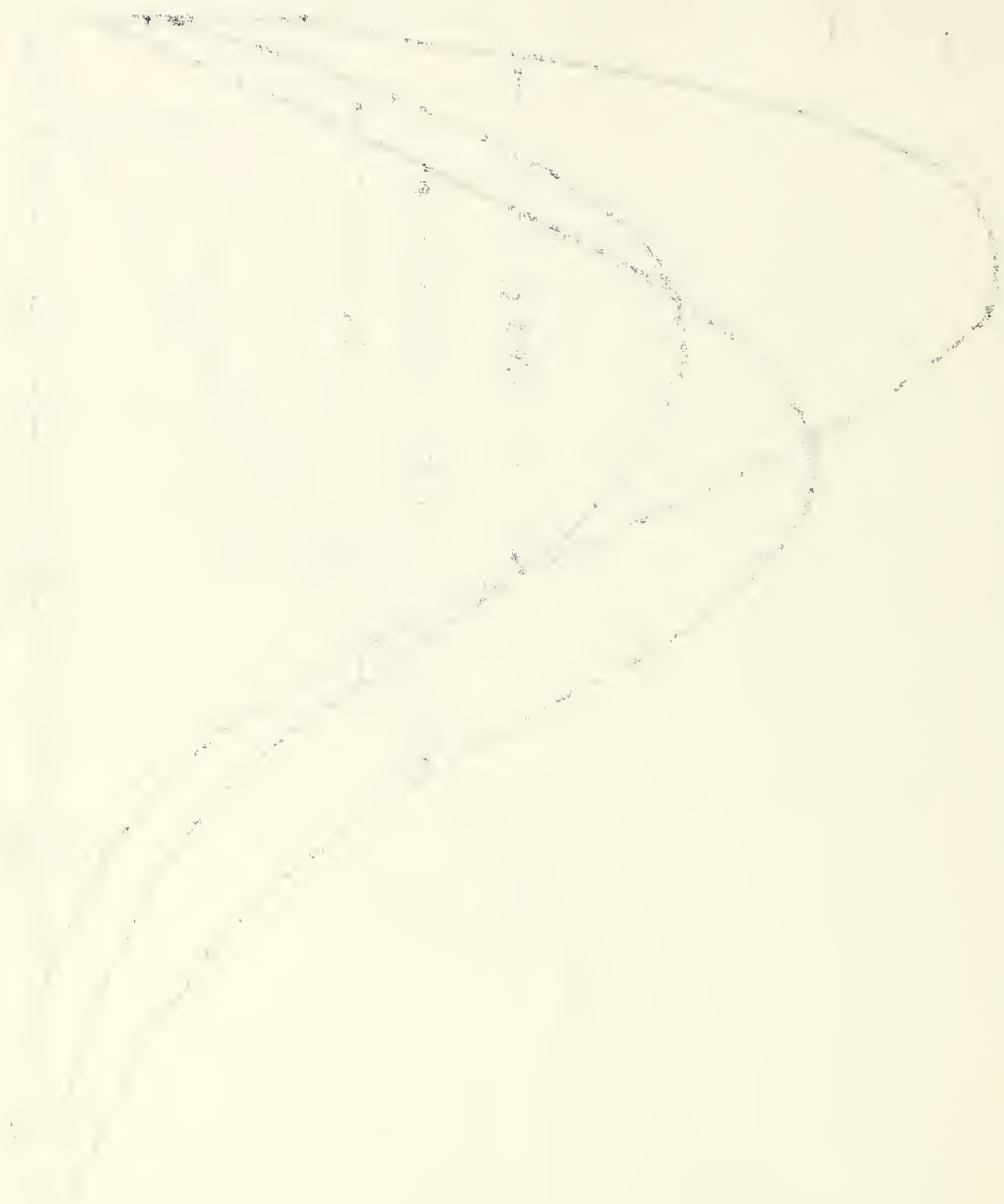


Fig. 9. The relative number of pulses in the end point channel as a function of the energy of the photon producing them for the incident bremsstrahlung spectrum and for the scattered spectra having rising and falling cross sections.



Photon Scattering and Self Absorption in Lead and Bismuth at 7 Mev.

E. G. Fuller and Evans Hayward
National Bureau of Standards
Washington 25, D. C.

It has already been shown¹ that the elastic scattering cross sections

1. E. G. Fuller and E. Hayward, Phys. Rev. 101, 692 (1956).

for many nuclei have two maxima. The higher energy peak can be related to the absorption of photons into the giant resonance; the lower energy peak, located just below the particle threshold, is associated with the absorption of photons into discrete levels. The scattering from some of these levels has recently been observed² using the six and seven Mev photons generated in

2. S.A.E. Johansson, Bull. Am. Phys. Soc. II, 3, 174 (1958).

K. Reibel and A. K. Mann, Bull. Am. Phys. Soc. Ser II, 3, 174 (1958).

the $F^{19}(p, \alpha \gamma)O^{16}$ reaction. This note contains further data obtained for the lower energy region using lead, radiopb, and bismuth scattering targets. These results were obtained from two types of measurements, the first a detailed determination of the elastic scattering cross section from four to ten Mev and the second a series of self-absorption measurements.

The resulting scattering cross sections were essentially the same as those obtained earlier. The values of the scattering cross section at its peak, σ_s^{\max} , and the integrals, $\int_0^{7.5} \sigma_s(E) dE$ are given in rows (1) and (2) of Table 1.

The self-absorption experiments consisted of measuring the attenuation of the scattered photons when an absorber of the target material was placed in the incident 7.5 Mev bremsstrahlung beam. The scattered photons were detected by a NaI(Tl) spectrometer and the pulses registered above a bias

[The text on this page is extremely faint and illegible. It appears to be a standard page of prose with several paragraphs of text.]

corresponding to four Mev were used to determine the attenuation. By weighting the bremsstrahlung spectrum with the elastic scattering cross section, it was found that the average energy for the photons scattered was six Mev. Table II shows the observed attenuations divided by $e^{-\mu_e \Delta}$ to correct for electronic absorption in the absorber. Transmissions significantly different from one represent absorption by nuclear energy levels, the magnitude of the effect depending on the average peak absorption cross section in the levels. The maximum absorption cross section in a given level is given by $2\pi \lambda^2 (2J + 1)/(2I + 1)$ where I is the spin of the ground state and J is the spin of the excited state. The average value of this cross section consistent with the dipole selection rule and averaged over the product of the scattering cross section and the bremsstrahlung spectrum are given in Table I. Since this peak cross section may be depressed by inelastic scattering or thermal Doppler broadening, the self-absorption experiment was also done with the targets and absorbers at liquid nitrogen temperature. The results indicate that the levels participating in radiolead are narrow compared to the Doppler width of 3 ev; whereas those in natural lead are wider. The bismuth data are inconclusive.

A calculation³ has been made of the expected transmission as a function

3. E. Hayward and E. G. Fuller, Phys. Rev. 106, 991 (1957).

of level width and peak absorption cross section assuming the scattering to result from a single average Doppler-broadened, Breit-Wigner level. Rows (4) and (5) of Table I give the range of values obtained for the average ground-state branching ratios and level widths consistent with the attenuations measured at 300° and 77°K. The summed ground-state widths obtained by



combining the latter with $\int_4^{7.5} \sigma_s(E) dE$ are shown in row (6).

The data in Table II also indicate that the photons scattered by a bismuth target can be removed by a lead absorber, though the converse is not observed. A reasonable explanation of this effect is that the scattering cross section in Bi is the result of the presence of a relatively small number of levels and that one of the stronger of these overlaps a level in lead. Experiments using absorbers enriched in Pb^{207} and Pb^{208} indicated definitely that a level in Pb^{208} is responsible, though the possibility that one in Pb^{207} also contributes to the absorption is not excluded. A further indication of the presence of one rather strong level in bismuth is the fact that the same attenuation was observed for two different thicknesses of bismuth absorber. This result is inconsistent with the calculated attenuation curves and suggests that the assumption that all the levels responsible for the bismuth scattering are alike is not valid. If about 70 percent of the photons scattered by bismuth do not self-absorb, then the observed attenuations can be understood. The attenuations obtained using a lead target and two lead absorber thicknesses are, on the otherhand, consistent with the simple picture.

TABLE I

	Pb	Pb^{206}	Bi
(1) $\langle \sigma_s \rangle^{\max}$ mb (7 Mev)	21	20	21
(2) $\int_4^{7.5} \sigma_s(E) dE$ Mev mb	42	40	48
(3) σ_a^0 barns	215	235	79
(4) $\Gamma_{g.s.}/\Gamma$	0.06 - 0.12	0.20 - 1.0	0.12 - 1.0
(5) Γ_{ev}	>3.1	0.2 - 3.1	>0.5
(6) $\sum \Gamma_{g.s.}$ ev	1100 - 2300	115 - 590	458 - 3800



TABLE II.

Observed Transmissions Corrected for Electronic Absorption.

Absorber	Thickness	Targets		
		Pb(7.2 g/cm ²)	Pb ²⁰⁶ (3.6g/cm ²)	Bi(3.97g/cm ²)
Pb	10.8 g/cm ²			0.895 ± 0.031
	14.4	0.663 ± 0.032	0.846 ± 0.019	
		0.694 ± 0.037*		
"Pb ²⁰⁶ "	11.2	0.976 ± 0.050	0.74 ± 0.043	1.002 ± 0.048
			0.599 ± 0.031*	
Bi	12.2	1.018 ± 0.050	1.045 ± 0.038	0.792 ± 0.040
				0.719 ± 0.038*
Pb	7.65	0.822 ± 0.029		0.903 ± 0.028
"Pb ²⁰⁸ "	7.83	0.790 ± 0.028		0.910 ± 0.028
"Pb ²⁰⁷ "	7.86	0.797 ± 0.028		0.915 ± 0.028
"Pb ²⁰⁶ "	7.47			0.965 ± 0.029
Bi	7.49			0.790 ± 0.025
Pb	52% Pb ²⁰⁸ ; 21% Pb ²⁰⁷ ; 26% Pb ²⁰⁶			
"Pb ²⁰⁶ "	3% Pb ²⁰⁸ ; 9% Pb ²⁰⁷ ; 88% Pb ²⁰⁶			
"Pb ²⁰⁷ "	31.3% Pb ²⁰⁸ ; 63.6% Pb ²⁰⁷ ; 5.1% Pb ²⁰⁶			
"Pb ²⁰⁸ "	96% Pb ²⁰⁸ ; 2.8% Pb ²⁰⁷ ; 1.2% Pb ²⁰⁶			

*Measured with both target and absorber at liquid nitrogen temperature.

The first part of the document discusses the importance of maintaining accurate records of all transactions. It emphasizes that every entry should be supported by a valid receipt or invoice. This ensures transparency and allows for easy verification of the data.

In the second section, the author outlines the various methods used to collect and analyze the data. This includes both primary and secondary data collection techniques. The primary data was gathered through direct observation and interviews with key personnel. Secondary data was obtained from existing reports and databases.

The third section details the statistical analysis performed on the collected data. Various statistical tests were used to determine the significance of the findings. The results indicate a strong correlation between the variables being studied, suggesting that the observed trends are not merely coincidental.

Finally, the document concludes with a series of recommendations based on the research findings. These recommendations are aimed at improving the efficiency of the processes being analyzed and ensuring that the organization remains competitive in its market.

Elastic Scattering of Photons by Tantalum^{*}

by

E. G. Fuller and Evans Hayward
National Bureau of Standards
Washington, D. C.

The neutron yield cross section for the deformed nucleus Ta¹⁸¹ has recently been measured^{1,2/} and found to consist of two maxima at

1/
E. G. Fuller and M. Weiss, Phys. Rev. to be published.

2/
Spicer et al., private communication.

12.45 and 15.45^{1/}. This cross section has been fitted by the superposition of two Lorentz lines. These have been associated with oscillations of the nuclear charge along the one long and two short axes of the ellipsoid according to the suggestions of Okamoto^{3/} and Danos^{4/}.

3/
K. Okamoto, Phys. Rev. 110, 143(1958).

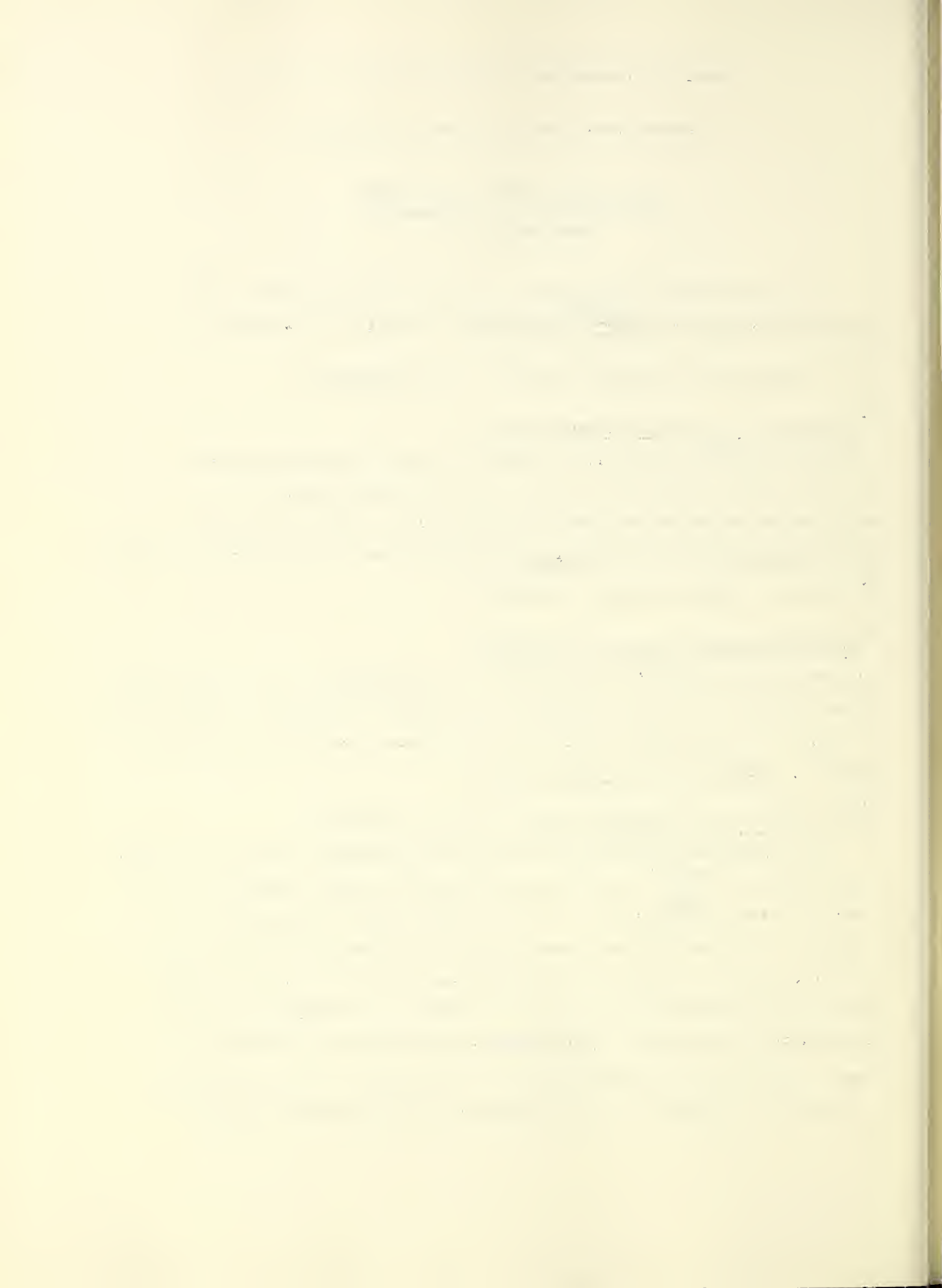
4/
M. Danos, Nuclear Physics 5, 23(1958).

The present note describes the results of a measurement of the differential cross section at 120° for the elastic scattering of photons by the tantalum nucleus. The experimental methods employed were described in a previous paper^{5/}. The results are given in Fig. 1.

5/
E. G. Fuller and E. Hayward, Phys. Rev. 101, 692(1956).

For comparison with these results the differential elastic scattering cross section, $\frac{d\sigma_s(\theta)}{d\Omega_e r}$, associated with electric dipole absorption, has been calculated assuming (a) that the nuclear dipole polarizability is a tensor, i.e. that the polarizability has a different value associated with the major and minor axes of the nucleus; and (b) that the nuclear dipole polarizability is a scalar, i.e. that it is independent of the orientation of the nucleus with respect to the photon polarization.

* This research was supported by the U. S. Air Force, through the Office of Scientific Research of the Air Research and Development Command.



In terms of the forward scattering amplitude, f , the relationships between the photon absorption and elastic scattering cross section, σ and σ_s , are:

$$\sigma = 4\pi k \text{Im } f$$

$$\frac{d\sigma_s(0^\circ)}{d\Omega} = |f|^2 \quad (1)$$

Whenever σ can be represented by a Lorentz line, and the nuclear polarizability associated with σ is along the direction of polarization of the incident photon, the forward scattering amplitude is given by:

$$f = \frac{\sigma_0 \Gamma}{4\pi \hbar c} \frac{E^2 (E_0^2 - E^2) + i E^3 \Gamma}{(E_0^2 - E^2)^2 + E^2 \Gamma^2} \quad (2)$$

where σ_0 is the peak absorption cross section, E_0 the resonance energy, and Γ the full width at half maximum of the resonance.

Assuming a tensor electric dipole polarizability, the scattering amplitude for a given nuclear axis, z , arbitrarily oriented with respect to the polarization of the incident photon is,

$$f(\theta) = f_z \cos \eta \sin \rho, \quad (3)$$

where θ is the scattering angle, η is the angle between the photon's polarization and z , ρ is the angle between z and the direction of observation, and f_z is given by Eq. (2) where the resonance parameters associated with the absorption of photons polarized along z are used. Danos has shown that, for an ellipsoidal nucleus, the relationship between the cross sections σ_a and σ_b associated with the absorption of photons polarized along the major and minor axes, and the total absorption cross section for an unpolarized photon beam by an unoriented sample is:

$$\sigma = \sigma_a/3 + 2 \sigma_b/3 \quad (4)$$

THE UNIVERSITY OF CHICAGO
DIVISION OF THE PHYSICAL SCIENCES
DEPARTMENT OF CHEMISTRY

REPORT OF THE
COMMISSION ON THE ORGANIZATION
OF THE DEPARTMENT OF CHEMISTRY

PRESENTED TO THE
FACULTY OF THE DIVISION OF THE PHYSICAL SCIENCES
AND THE BOARD OF THE DIVISION OF THE PHYSICAL SCIENCES

BY
THE COMMISSIONERS
J. H. COOPER, CHAIRMAN
AND
J. H. COOPER, MEMBER

CHICAGO, ILLINOIS
1954

THE UNIVERSITY OF CHICAGO
DIVISION OF THE PHYSICAL SCIENCES
DEPARTMENT OF CHEMISTRY

REPORT OF THE
COMMISSION ON THE ORGANIZATION
OF THE DEPARTMENT OF CHEMISTRY

PRESENTED TO THE
FACULTY OF THE DIVISION OF THE PHYSICAL SCIENCES
AND THE BOARD OF THE DIVISION OF THE PHYSICAL SCIENCES

BY
THE COMMISSIONERS
J. H. COOPER, CHAIRMAN
AND
J. H. COOPER, MEMBER

CHICAGO, ILLINOIS
1954

For such an ellipsoidal nucleus the scattering cross section at an angle θ will be given by the absolute square of the sum of the scattering amplitudes associated with the three orthogonal nuclear axes, averaged over all orientations of the nucleus with respect to the incident photon's polarization and finally averaged over all polarizations of the photon. If A and α , B and β , are the real and imaginary parts of the scattering amplitudes associated with σ_a and σ_b , and D is the nuclear Thomson scattering amplitude, $-Z^2 e^2 / Amc^2$, the resulting expression for the differential scattering cross section is:

$$\frac{d\sigma_s(\theta)}{d} = \frac{3}{15} (A^2 + \alpha^2) + \frac{11}{30} (B^2 + \beta^2) - \frac{1}{15} (AB + \alpha\beta) + \frac{1}{3} AD + \frac{2}{3} BD + \frac{1}{2} D^2 + \left[\frac{1}{15} (A^2 + \alpha^2) + \frac{7}{30} (B^2 + \beta^2) + \frac{1}{5} (AB + \alpha\beta) + \frac{1}{3} AD + \frac{2}{3} BD + \frac{1}{2} D^2 \right] \cos^2 \theta \quad (5)$$

If, on the other hand, the two resonances found for the neutron yield cross sections for tantalum are not associated with different axes, i.e. if the nuclear polarizability is assumed to be a scalar, the dipole moment induced in the nucleus is always along the polarization of the incident photon. The scattering amplitude for the two resonances is then the sum of the amplitudes for the two resonances with an angular dependence determined by the sine of the angle between the polarization of the incident photon and the direction of observation. The differential scattering cross section is then given by the average of the absolute square of this scattering amplitude over all orientations of the photon's polarization:

$$\frac{d\sigma_s(\theta)}{d\Omega} = \frac{1 + \cos^2 \theta}{2} \left[\left(\frac{A + 2B}{3} + D \right)^2 + \left(\frac{\alpha + 2\beta}{3} \right)^2 \right] \quad (6)$$

where $A/3$, $2B/3$, $\alpha/3$ and $2\beta/3$ are the real and imaginary parts of the forward scattering amplitudes associated with the two resonances found in the absorption cross section.

1. The first part of the document discusses the importance of maintaining accurate records of all transactions. It emphasizes that proper record-keeping is essential for the integrity of the financial system and for the ability to detect and prevent fraud. The text notes that without reliable records, it would be difficult to track the flow of funds and identify any irregularities.

2. The second part of the document outlines the specific procedures for recording transactions. It details the steps involved in entering data into the system, including the use of standardized codes and the requirement for double-checking entries. The text also mentions the importance of regular audits to ensure the accuracy of the records.

3. The third part of the document discusses the role of the accounting department in maintaining these records. It highlights the need for clear communication and collaboration between different departments to ensure that all transactions are properly recorded and reported. The text also mentions the importance of staying up-to-date on changes in accounting standards and regulations.

4. The fourth part of the document discusses the use of technology in record-keeping. It notes that modern accounting systems can greatly improve the efficiency and accuracy of the process. However, it also emphasizes the need for proper training and security measures to protect the data from unauthorized access or loss.

5. The fifth part of the document discusses the importance of transparency and accountability in financial reporting. It notes that clear and accurate records are essential for providing stakeholders with reliable information about the organization's financial performance. The text also mentions the need for regular communication and reporting to build trust and confidence.

6. The sixth part of the document discusses the role of the internal control system in maintaining accurate records. It notes that a strong internal control system can help to prevent errors and fraud, and ensure that all transactions are properly recorded and reported. The text also mentions the importance of regular reviews and updates to the control system.

7. The seventh part of the document discusses the importance of documentation and archiving of records. It notes that all records should be properly stored and backed up to ensure their long-term availability. The text also mentions the need for a clear policy regarding the retention and disposal of records.

8. The eighth part of the document discusses the importance of staying up-to-date on changes in accounting standards and regulations. It notes that the accounting profession is constantly evolving, and it is essential for organizations to stay current on the latest developments. The text also mentions the need for ongoing training and education for accounting staff.

9. The ninth part of the document discusses the importance of maintaining accurate records for legal and regulatory compliance. It notes that many organizations are required to maintain certain records for a specific period of time, and failure to do so can result in penalties and legal action. The text also mentions the need for a clear policy regarding record retention and disposal.

Equations (5) and (6), evaluated at 120° and using the parameters of reference 1, are plotted in Fig. 1. The cross section obtained from the scalar expression (Eq. 6) shows the effects of strong destructive interference between the two resonances. This interference is essentially missing in the tensor polarizability case since the absorption is now associated with the orthogonal axes of the nucleus. The experimental cross section as a function of energy is in better agreement with the result calculated from the tensor expression than that obtained assuming a scalar polarizability. This result tends to confirm the spatial correlation of the dipole polarizability for a deformed nucleus as proposed by Danos and Okamoto.

In order to achieve the agreement in magnitude displayed in Fig. 1, the peak cross sections of the resonances of reference 1 were reduced by 10%. Since the absolute cross sections of reference 1 are known to only about 15% and since there are possible systematic errors (as large as $\pm 7\%$) in the absolute magnitude of the scattering cross section, this adjustment is well within the errors in the absolute sizes of the two cross sections being compared. The difference between the experimental points and the smooth curve at the higher energies is probably significant. It represents more absorption than is given by the two Lorentz lines used to predict the scattering cross section. The neutron yield cross section of reference 1 is also higher than the Lorentz lines in this energy region.

The authors want to thank M. Danos for his help in understanding these results.



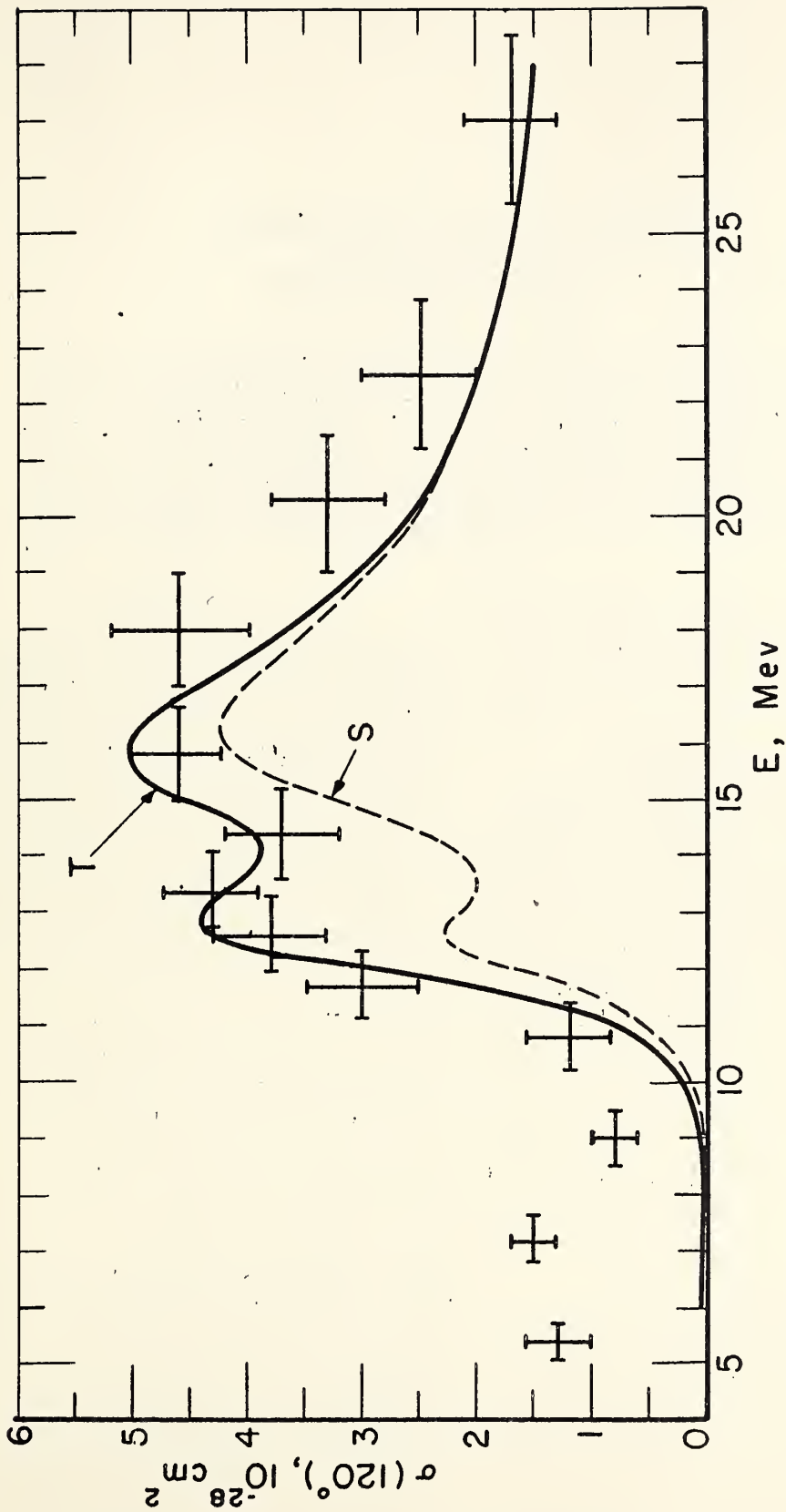


Fig. 1. The differential elastic scattering cross section for tantalum at 120° as a function of photon energy. The smooth curves are calculated using the dispersion relation and the resonance parameters given in reference 1 with the peak cross sections reduced by 10%. The solid curve is the result obtained assuming a tensor electric dipole polarizability (Eq. 5); whereas the dashed curve results from assuming a scalar polarizability (Eq. 6).

1000



Nuclear Elastic Scattering of Photons*

E. G. FULLER AND EVANS HAYWARD
National Bureau of Standards, Washington, D. C.
(Received September 16, 1955)

A NaI(Tl) scintillation spectrometer biased to detect only photons in the upper energy tip of a betatron-produced bremsstrahlung spectrum is used to measure the differential nuclear elastic scattering cross section at 120 degrees as a function of photon energy from 4 to 40 Mev. The targets ranged in Z from Na to U. Total cross sections are calculated by assuming a dipole angular distribution. The scattering cross sections tend to exhibit two maxima, one below the particle threshold that corresponds to the scattering by separate levels, and one that follows the giant resonance for photon absorption. Both the maximum cross section and the energy of the giant resonance vary smoothly with A from Na to U and are roughly proportional to $(NZ/A)^2$ and $A^{-1/3}$, respectively. The dipole dispersion relation is used to compare the scattering data with the neutron yield data in the giant resonance region.

I. INTRODUCTION

THE absorption of gamma rays by nuclei has been the subject of numerous investigations. The most recent compilations of experimental data are those given by the Saskatchewan¹ and Pennsylvania² groups. Most of this work has involved the measurement of neutron emission cross sections which, when integrated over the "giant resonance," have been compared to the predictions of the dipole sum rule. The elastic scattering process associated with the nuclear absorption of photons presents an alternative way of studying the basic interaction. This paper is an account of an experimental study of the elastic scattering cross section as a function of both energy and atomic number.³ The results are compared with the neutron yield cross sections.

The scattering of photons in the region of the "giant resonance" was probably first observed by Gaerttner and Yeater⁴ and Dressel, Goldhaber, and Hanson.⁵ In a more refined experiment⁶ Stearns studied the scattering of the $\text{Li}(p,\gamma)$ photons by various nuclei using a

NaI(Tl) scintillation counter which detected only the elastically scattered photons. The results indicated that the cross section for the elastic scattering of 17-Mev photons by heavy nuclei is of the order of a few millibarns.

II. EXPERIMENTAL METHOD

The present experiment is an extension of the Stearns experiment. The discrimination level of a large NaI(Tl) scintillation spectrometer is set to detect only the photons in the upper energy tip of the betatron bremsstrahlung spectrum. The spectrometer is first calibrated at a given energy by observing the number of counts, C_1 , produced when the spectrometer is placed in the direct beam from the betatron (see Fig. 1). Simultaneously a charge, Q_1 , is collected from a transmission ionization chamber in the direct beam. With the detector rotated to the 120° position the number of counts, C_2 , produced by scattered photons is recorded while a charge, Q_2 , is collected from the ionization chamber. On the assumption that the shape of the bremsstrahlung spectrum is the same for both the high and low intensity beams, the elastic scattering cross section is then given by:

$$\langle \sigma_s \rangle_{Av} = K(C_2/Q_2) \cdot (Q_1/C_1), \quad (1)$$

where K includes geometrical factors as well as a correction for the absorption of photons in the target. The scattering cross section was determined as a function of energy from 4 to 40 Mev by changing both the peak energy of the betatron and the gain of the amplifier so as to keep the end of the bremsstrahlung spectrum at the same discrimination level. The measured cross

* This research was supported by the U. S. Air Force, through the Office of Scientific Research of the Air Research and Development Command.

¹ Montalbetti, Katz, and Goldemberg, Phys. Rev. 91, 659 (1953); Summers-Gill, Haslam, and Katz, Can. J. Phys. 31, 70 (1953); J. Goldemberg and L. Katz, Can. J. Phys. 32, 49 (1954).

² R. Nathans and J. Halpern, Phys. Rev. 93, 437 (1954); R. Nathans and P. F. Yergin, Phys. Rev. 98, 1296 (1955).

³ E. G. Fuller and E. Hayward, Phys. Rev. 94, 732 (1954); 95, 1106 (1954); *Proceedings of the 1954 Glasgow Conference* (Pergamon Press, New York, 1955), pp. 155-161. The cross sections given in the present paper differ from those previously published because of an improved estimate of the solid angle.

⁴ E. R. Gaerttner and G. L. Yeater, Phys. Rev. 76, 363 (1949).

⁵ Dressel, Goldhaber, and Hanson, Phys. Rev. 77, 754 (1950).

⁶ M. B. Stearns, Phys. Rev. 87, 706 (1952).

sections are independent of both the shape of the bremsstrahlung spectrum and the response of a monitor.

III. APPARATUS

The physical layout of the experiment is shown in Fig. 1. The repetition rate of the betatron is 180 cycles per second. As operated for this experiment the yield pulse was approximately triangular in shape with a base length of about $10 \mu\text{sec}$. The energy to which the electrons in the betatron are accelerated is controlled by a circuit that uses a dc biased peaker transformer to determine when the current in the main coil of the betatron reaches a predetermined value. The energy scale was determined in a separate experiment by observing the (γ, n) thresholds in Be^9 at 1.67 Mev, B^{10} at 8.45 Mev, Cu^{65} at 9.9 Mev, and Cu^{63} at 10.7 Mev. Within the errors of the end-point determinations made during this experiment ($\pm 5\%$), a linear extrapolation of this energy calibration to 40 Mev appears to be valid.

The output from the betatron was monitored by measuring the charge collected from the parallel plate ionization chamber on a polystyrene film condenser. The voltage to which this condenser was charged was measured with a vibrating reed electrometer (Applied Physics Corporation Model 30). To cover the range of beam intensities used, any one of four charge collecting condensers could be switched into the circuit. These ranged in value from about 5.0 to 0.005 microfarads. The ratio of the capacities of these condensers was determined by measuring the time taken for each of

them to charge to a given voltage when a radioactive source was placed in a standard position with respect to the chamber. The ionization chamber was checked for saturation effects; none were observed at the highest intensities obtained with the betatron.

The beam was defined by a collimating hole one and one-half inches in diameter through eight inches of lead. This produced a beam four inches in diameter at the target position. The collimating hole was filled with a low- Z material, usually aluminum,⁷ to remove preferentially low-energy photons from the bremsstrahlung spectrum.

The detector⁸ was a large NaI(Tl) crystal five inches in diameter and four inches long viewed by a Dumont K1198 photomultiplier tube. The crystal, photomultiplier, and cathode follower were all located in a lead container having walls five inches thick surrounded with boxes filled with a mixture of boric acid and paraffin. The counter and its shielding were on a table that could be rotated about a vertical axis through the target position. The crystal viewed the target through a hole five inches in diameter in the shield. This hole contained an aluminum plug four and one-half inches long which filtered out electrons and low-energy photons emitted by the target.

The pulses from the cathode follower were fed by a long cable into the betatron control room where they were amplified and analyzed by a five-channel integral discriminator (Channels *A* through *E*) and two differential discriminators (*F* and *G*). The amplifier and discriminators were all of conventional design. The outputs of the discriminators were gated so that only those events occurring in a $20\text{-}\mu\text{sec}$ interval around the betatron yield pulse were counted. With this gating the cosmic-ray background was of the order of $\frac{1}{3}$ count per hour in the differential channels. The maximum counting rate in these channels due to photons scattered from the sample was of the order of 20 counts per hour. This rate was limited by the duty cycle of the betatron.

The biases at which the various discriminators were set are indicated in Fig. 2. Also shown in this figure are the pulse-height distributions obtained in the direct beam from the betatron and in the beam scattered by an Al target. At each energy at which measurements were made the detector was first swung into the direct betatron beam and the amplifier gain adjusted until the end point of the pulse-height spectrum produced by the filtered bremsstrahlung beam fell into the differential channel *G*. The counts registered by *F*, called the end-point channel, were then used to calculate the elastic scattering cross sections. The other channels, biased above and below *F*, were useful in monitoring the stability of the equipment and pileup. In all runs the counting rate of discriminator *A* was used to set the output intensity of the betatron. Pileup in *F* was experi-

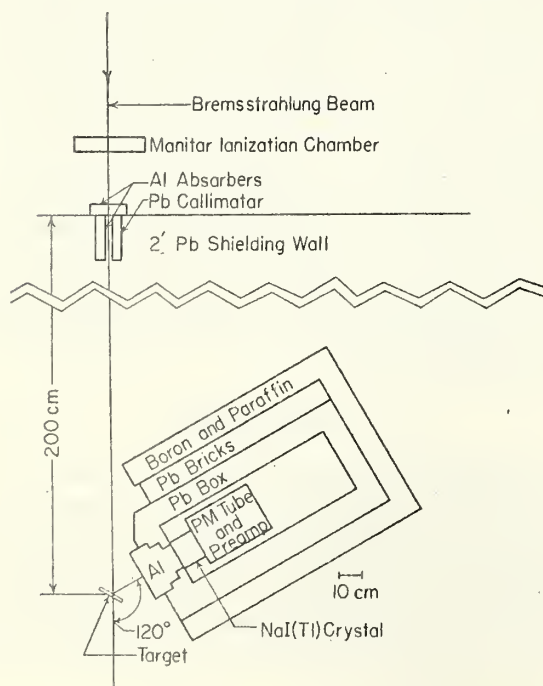


FIG. 1. The experimental arrangement. The detector rotates about a vertical axis through the sample.

⁷ The scattering cross section for Al was measured with a carbon beam filter.

⁸ R. S. Foote and H. W. Koch, Rev. Sci. Instr. 25, 746 (1954).

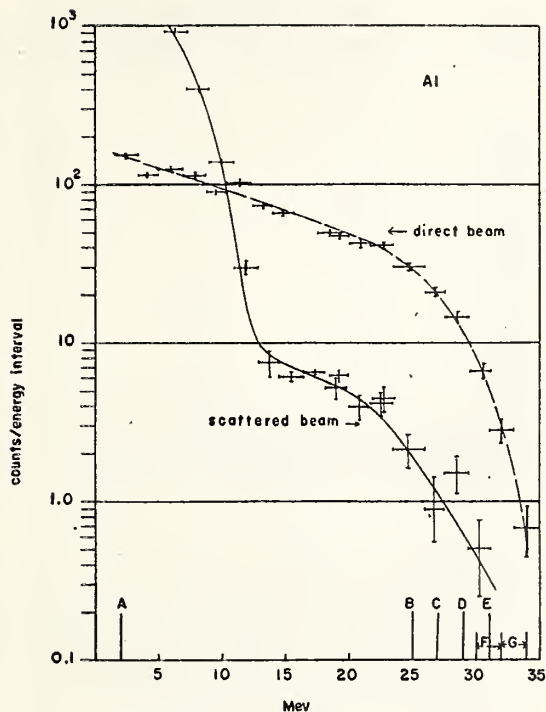


FIG. 2. The pulse-height distributions obtained when the detector is placed in the filtered bremsstrahlung beam and in the beam scattered by an Al target. The peak energy of the betatron was 33 Mev. The levels at which the discriminators fired are indicated by the vertical lines at the bottom. A through E were integral discriminators, and F and G differential discriminators. F is the channel used to determine the elastic scattering cross sections. The sharp rise in the pulse-height spectrum below 12 Mev may probably be attributed to photons resulting from the capture of fast neutrons generated in the target.

mentally found to be negligible if the counting rates in A were kept below 10 per second and 60 per second for runs made in the direct and scattered beams, respectively.

The energy assignment of each measurement was made on the basis of the betatron energy calibration. The firing point of each of the discriminators was first determined with a precision pulser. On the basis of the observed pulse-height distributions in the end-point runs for a particular energy E_0 , a pulse-height was assigned to E_0 . This pulse height was slightly higher than the firing point of the lower edge of discriminator G. A linear extrapolation was then made to determine the energies to be assigned to the edges of the end-point channel, F. It is felt that these energy assignments are probably good to about 5%.

IV. ANALYSIS OF THE DATA

In order to calculate the cross section, the quantity K in Eq. (1) must be evaluated. Since the targets are of the order of a mean free path thick, a correction for the absorption by the target of photons in both the incident and the scattered beams must be made. The "electronic" absorption processes (i.e., pair production,

Compton effect, and photoelectric effect) account for most of this absorption although in some cases it is also necessary to include the effect of the nuclear absorption. In the region of the giant resonance the nuclear absorption cross sections are only a few percent of the "electronic" absorption cross sections and need not be considered.

In the energy region just below the particle thresholds, the observed scattering is presumably due to sharp, well-defined levels. For the lighter nuclei particularly, the maximum nuclear absorption cross section in these levels can reach values of the order of, or possibly greater than, the "electronic" absorption cross section. The maximum value of the dipole absorption cross section in an individual level is $6\pi\lambda^2$. For a 7-Mev photon this gives a cross section of about 100 barns. In any actual case this maximum value will be reduced because of inelastic scattering and the thermal Doppler broadening of the level. Experiments on neutron capture and scattering⁹ indicate that the radiation widths, Γ_γ , of nuclear energy levels at excitations of 7 Mev or so are a few tenths of an electron volt. The thermal Doppler width, δ , of a level for 7-Mev photons ranges from 10 electron volts for $A=25$, to 3.6 electron volts at $A=208$. The maximum absorption cross section in the levels is therefore determined chiefly by the Doppler broadening and is given by $\sigma_{\max} \approx 6\pi\lambda^2\Gamma_\gamma/\delta = 1$ barn for nuclei around Mg. This cross section is of the same order as the "electronic" absorption cross section in Mg and therefore contributes appreciably to the absorption of photons in the scattering target.

The effect of absorption in the scattering target on the observed counting rate can be seen in the following way. Consider the scattering from the small element of the target dx as indicated in Fig. 3. The number of counts in the end-point channel from this element is then given by:

$$dC_2 = Q_2 \frac{C_1}{Q_1} \frac{N dx \Delta\Omega}{C_0 \delta} \int_E^{E+\Delta E} dE \frac{\sigma_e}{13.4} f(E) \times e^{-N x (\sigma_n + 2\sigma_e) / \cos\beta} / \int_E^{E+\Delta E} dE f(E). \quad (2)$$

In this expression N is the number of atoms per cm^3 in the target, $\Delta\Omega$ is the average solid angle for detecting a photon scattered by the target, σ_e is the total scattering cross section, σ_n is the nuclear absorption cross section, σ_e is the electronic absorption cross section, and $f(E)$ is the product of the incident photon spectrum and the response of the detector as a function of energy. If the variation of $f(E)$ across ΔE is neglected, Eq. (2) becomes:

$$dC_2 = Q_2 \frac{C_1}{Q_1} \frac{N dx \Delta\Omega}{C_0 \delta} \int_E^{E+\Delta E} dE \frac{\sigma_e}{13.4} e^{-N x (\sigma_n + 2\sigma_e) / \cos\beta}. \quad (3)$$

⁹ D. J. Hughes and J. A. Harvey, Nature 173, 942 (1954).

The number, 13.4, is the ratio of the total cross section to the differential cross section at 120 degrees for an angular distribution of the scattered radiation varying as $(1+\cos^2\theta)$. σ_e is included twice in the exponent of Eq. (2) since both the incident and scattered photon beams are absorbed by electronic processes. As was pointed out above, σ_n is comparable to σ_e only for the scattering by sharp, well-defined levels. In this case the Doppler shift in the photon energy, because of the recoil of the scattering nucleus (10^3 ev for a 7-Mev photon scattered by an Sn nucleus) is so large that it cannot be reabsorbed by the same level in the scattered beam. For this reason the nuclear absorption takes place in the primary beam only.

The solid angle for the detection of a scattered photon depends both on the position of the scattering nucleus within the target and on the depth, l , in the crystal at which the photon is absorbed. It was determined experimentally with a small point source that the mean solid angle averaged over the beam area on the front face of the target was given to a good approximation by the solid angle for detecting a photon scattered by a nucleus at the center of the beam. Neglecting the effect of the finite thickness of the target, the average solid angle for detecting a photon is then

$$\Delta\Omega = \frac{A}{R^2} \int_0^L \frac{e^{-\mu l} dl}{(R+l)^2} / \int_0^L \frac{e^{-\mu l} dl}{R^2}, \quad (4)$$

where L is the length of the crystal, A is its cross-sectional area, μ is the absorption coefficient of NaI(Tl), and R is the distance from the center of the target to the center of the front face of the crystal. $\Delta\Omega$ is approximately given by $0.82 A/R^2$ over the energy range from 4 to 40 Mev. The correction to the mean solid angle due to the finite thickness of the targets was calculated to be negligible for the heavy nuclei. For the lighter nuclei this effect decreased the mean solid angle by a maximum of 10% in the case of S. In Table I the properties of the various targets are listed along with

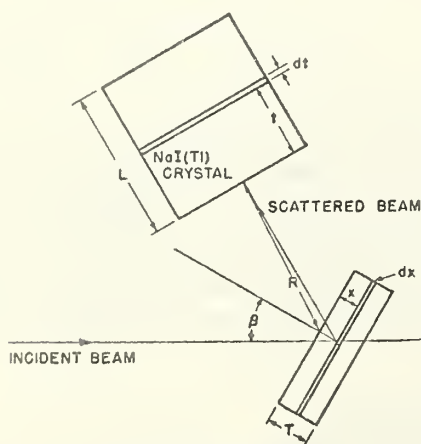


FIG. 3. The geometry.

TABLE I. Target properties.

	T g/cm ²	T cm	F^a
Na	7.1	6.7	0.91
Mg	8.85	5.1	0.93
Al	6.85	2.5	0.96
S	15.5	7.6	0.90
Ca	7.9	5.1	0.92
Mn	10.7	3.8	0.94
Ni	9.45	1.8	1.0
Cu	10.8	1.2	1.0
Sn	6.8	0.93	1.0
I	7.22	1.8	1.0
Au	26.1	1.35	1.0
Pb	14.4	1.27	1.0
Bi	12.3	1.27	1.0
U	26.3	1.42	1.0

^a F is the factor by which the mean solid angle for detecting a scattered photon is reduced due to the finite thickness of the scattering target (see text).

the correction, F , applied to the mean solid angle to take account of the finite target thickness.

In order to obtain an expression for an average scattering cross section Eq. (3) may be integrated through the target thickness and rearranged to give

$$\frac{C_2 Q_1}{C_1 \Delta\Omega \cos\beta} \frac{13.4}{\Delta E} = \frac{1}{\Delta E} \int_E^{E+\Delta E} \frac{\sigma_e}{\sigma_n + 2\sigma_e} dE \times [1 - e^{-NT(\sigma_n + 2\sigma_e)/\cos\beta}]. \quad (5)$$

Multiplying both sides by $2\sigma_e/[1 - e^{-2\sigma_e NT/\cos\beta}]$ yields

$$\frac{C_2 Q_1}{C_1 \Delta\Omega \cos\beta} \frac{13.4}{[1 - e^{-2\sigma_e NT/\cos\beta}]} \frac{2\sigma_e}{[1 - e^{-2\sigma_e NT/\cos\beta}]} = \langle \sigma_s \rangle_{Av} = [1 - e^{-2\sigma_e NT/\cos\beta}]^{-1} \frac{1}{\Delta E} \int_E^{E+\Delta E} \frac{\sigma_e}{1 + (\sigma_n/2\sigma_e)} dE \times [1 - e^{-NT(\sigma_n + 2\sigma_e)/\cos\beta}]. \quad (6)$$

If σ_n is small compared to $2\sigma_e$ as is true in the region of the giant resonance, $\langle \sigma_s \rangle_{Av}$ is just the scattering cross section averaged over the energy interval ΔE , since σ_e is a slowly varying function of the energy and can be taken outside the integral sign. If, on the other hand, σ_n is not negligible, as is sometimes the case below the particle thresholds, $\langle \sigma_s \rangle_{Av}$ will not be the average scattering cross section, since it does not include an adequate correction for self-absorption in the target. The magnitude of the additional correction for this effect can be obtained from a self-absorption experiment. Preliminary results¹⁰ indicate that in the energy region of the low-energy maximum (see Figs. 4-6) for Mn, Al, Ni, Bi, and Pb the average scattering cross section is approximately 15% higher than the values of $\langle \sigma_s \rangle_{Av}$ obtained from the left side of Eq. (5) and plotted in Figs. 4-6.

¹⁰ E. G. Fuller and E. Hayward, Phys. Rev. 98, 1537 (1955).

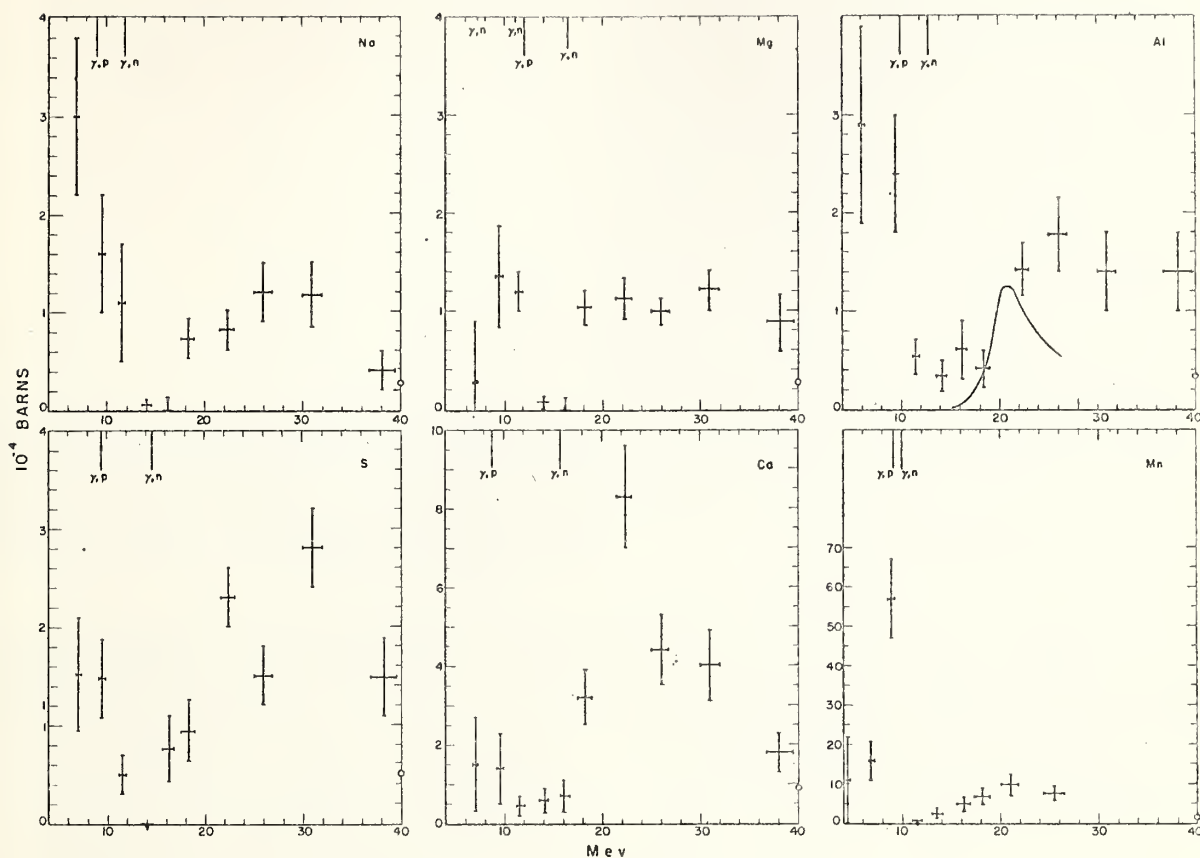


FIG. 4. The elastic scattering cross sections for Na, Mg, Al, S, Ca, and Mn. The indicated spread in energy is the width of the differential discriminator channel, and the standard deviations are based only on the number of counts. The vertical lines at the top represent the particle thresholds for the most important isotopes. The open circles at the extreme right indicate the magnitude of the Thomson cross section for Z free protons scattering coherently. The solid curve superimposed on the Al data is the scattering cross section calculated from the dispersion relation by substituting for $\sigma_a(E)$ in Eq. (6) the sum of the neutron and proton yield¹⁵ cross sections.

V. RESULTS AND DISCUSSION

The experimental results are plotted in Figs. 4–5. The indicated spread in energy is the width of the endpoint channel. The mean energy corresponding to each point is not necessarily at the center of the channel because of the variation of the scattering cross section, the response of the detector, and the incident photon spectrum over ΔE . The indicated uncertainties in the cross sections are the standard deviations based only on the number of counts. Systematic errors in the absolute cross sections may be as large as 15%. These would not affect the relative cross sections at different energies or for different elements. The largest uncertainty is probably in the estimate of the solid angle.

The measured elastic scattering cross sections are, of course, the result of the interference between the coherent processes, Rayleigh, Delbruck, nuclear resonant, and Thomson scattering. Since the present experiment was done at a backward angle, Rayleigh and Delbruck scattering, associated with electronic absorption processes, are negligible and only the scattering by the nuclear charge distribution need be considered. In

the low-energy limit this is just the Thomson scattering cross section for a rigid charge of mass A and charge Z , $(8\pi/3)(Z^2e^2/AMc^2)^2$. In the high-energy limit the cross section is that for Z free protons scattering coherently, i.e., the scattering by a rigid charge of mass Z and charge Z , $(8\pi/3)(Ze^2/Mc^2)^2$. At intermediate energies the nuclear resonant scattering results from the elastic deformation of the nuclear charge distribution. The magnitude of the nuclear Thomson scattering cross section is usually small compared to the experimentally measured scattering but on the high side of the giant resonance, the scattering cross section may be approaching the Thomson cross section for Z free protons, indicated by the open circles on the right side of Figs. 4–6.

The measured elastic scattering cross sections all rise smoothly to a maximum above the particle emission thresholds of the scattering nuclei. For the lighter elements ($A < 50$) these maxima bear little resemblance to the giant resonance curves obtained from the photon-neutron experiments. For the heavier nuclei ($A > 50$), however, the scattering curves follow the trend of the

giant resonance obtained from the neutron emission experiments. The magnitude of the scattering cross section at the peak is a smooth function of A varying from 0.12 mb for Na to 15 mb for Pb. Many of the elements studied also have a secondary maximum in the cross section below the particle threshold where the scattering is comparable to that in the giant resonance region. The ratio, R , of the peak cross section in this low-energy maximum to that at the peak of the giant resonance is given in Table II. The wide variations in this ratio, in contrast to the smooth trend of the peak scattering cross section in the giant resonance, indicate that the scattering below the particle thresholds reflects individual nuclear properties rather than the gross properties of nuclear matter that describe the giant resonance.¹¹ These individual properties show up most markedly in the self-absorption experiment¹⁰ where the analysis of the data yields information about mean radiation widths and level densities.

The qualitative features of the scattering curves can be understood as follows: At excitations below the

TABLE II. Comparison of cross sections. R is the ratio of the peak cross section below the particle thresholds to that at the peak of the giant resonance. $\sigma(\gamma, n)$ and σ_s are the neutron yield cross section and the scattering cross section at the peak of the giant resonance, respectively. σ_T is $\sigma(\gamma, n)$ multiplied by the ratio of the total particle yield to the neutron yield. $6\pi\lambda^2$ is evaluated at the energy corresponding to the peak of the giant resonance.

	1 R	2 $\sigma^2(\gamma, n)/\sigma_s$ barns	3 σ_T^2/σ_s barns	4 $6\pi\lambda^2$ barns	Reference
Na	2.5				
Mg	1.0				
Al	1.6				
S	0.5				
Ca	0.2				
Mn	5.7	13.7		21	1
		14			2
Ni	2.8	2.5	10	22	1, 15
Cu	1.0	9.8	19	23	1, 16
Sn	3.8				
I	0.27	30		32	1
		8.5			2
Au	0.3	46.5		36	1
		19.3			2
Pb	1.2	53		44	1
		40			2
Bi	1.9	74		44	1
		35			2
U	0.3	40		40	2

¹¹ Since the capture of slow neutrons in the detector will produce photons of about 7 Mev, some consideration has been given to the possibility that some of the counts observed at this energy might result from neutron capture gamma rays. The counting rates with the sample removed from the x-ray beam were negligible so that background neutrons produced in the betatron and its shielding contributed little. With the scattering target in the beam the observed relative counting rates were consistent neither with the slow or fission neutron capture cross sections, nor with the fast neutron scattering cross sections for the target nuclei. Neutrons accompanying the x-ray beam captured in the target, or scattered into the detector by the target, probably then contribute a negligible amount to the observed counting rate. In the case of Sn and Pb the observed low-energy maximum in the scattering cross section is at an energy slightly above the (γ, n) threshold for about 20% of target nuclei. Extremely rough estimates indicate that no more than 15% of the counting rate from Sn and Pb resulted from photoneutrons produced in the scattering target.

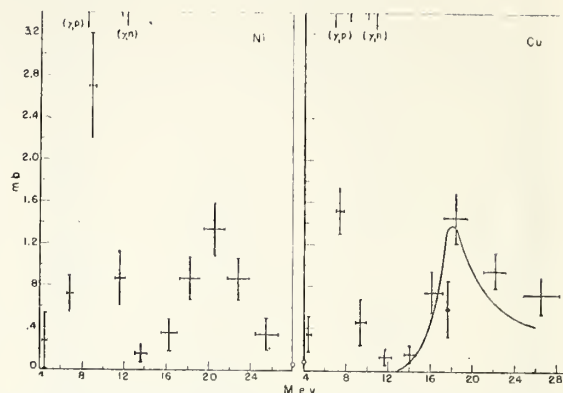


Fig. 5. The elastic scattering cross sections for Ni and Cu. The point at 17.6 Mev is that of Starns.⁶ The solid curve superimposed on the Cu data is the scattering cross section calculated from the dispersion relation by substituting for $\sigma_a(E)$ in Eq. (7) the (γ, n) cross section¹ multiplied by the ratio of the total particle yield to the neutron yield.¹⁶ The open circles on the vertical axes indicate the magnitude of the Thomson cross section for Z free protons scattering coherently.

particle thresholds the nucleus can lose its energy only by photon emission, either by a transition directly to the ground state or by transitions to intermediate states. The size of the low-energy maximum in the scattering cross section then depends in part on the number of alternative modes of decay available for the excited nucleus and therefore on the details of the level structure in the particular scattering nucleus. As the energy of excitation is increased above the particle threshold the scattering cross section drops sharply because of competition with particle emission. This result is in agreement with the qualitative prediction of Bethe and Ashkin.¹² At still higher energies the average ratio of photon emission to particle emission becomes constant and the cross section rises again to follow the trend of the oscillator strength distribution in the giant resonance.

The shape of the elastic scattering cross section in the giant resonance region may be compared with the shape of the cross section for neutron production obtained from other betatron experiments. For the heavier elements, $A > 50$, the widths and positions of the peaks of the cross sections displayed in Figs. 4-6 are very similar to the corresponding quantities obtained from the neutron yield cross sections. For the lighter nuclei, $A < 50$, however, the scattering cross section curves are considerably broader and peak at much higher energies than would be suggested by the neutron yield data.^{1,2,13} For example, the neutron yields cross section for aluminum peaks near 20 Mev, and has a width of about 2 Mev; whereas the elastic scattering cross section has a broad maximum located near 28 Mev. The energy that corresponds to the center of the oscillator strength

¹² H. Bethe and J. Ashkin, *Experimental Nuclear Physics*, edited by E. Segrè (John Wiley and Sons, Inc., New York, 1953), Vol. 1, p. 347.

¹³ Ferguson, Halpern, Nathans, and Yergin, *Phys. Rev.* 95, 776 (1954).

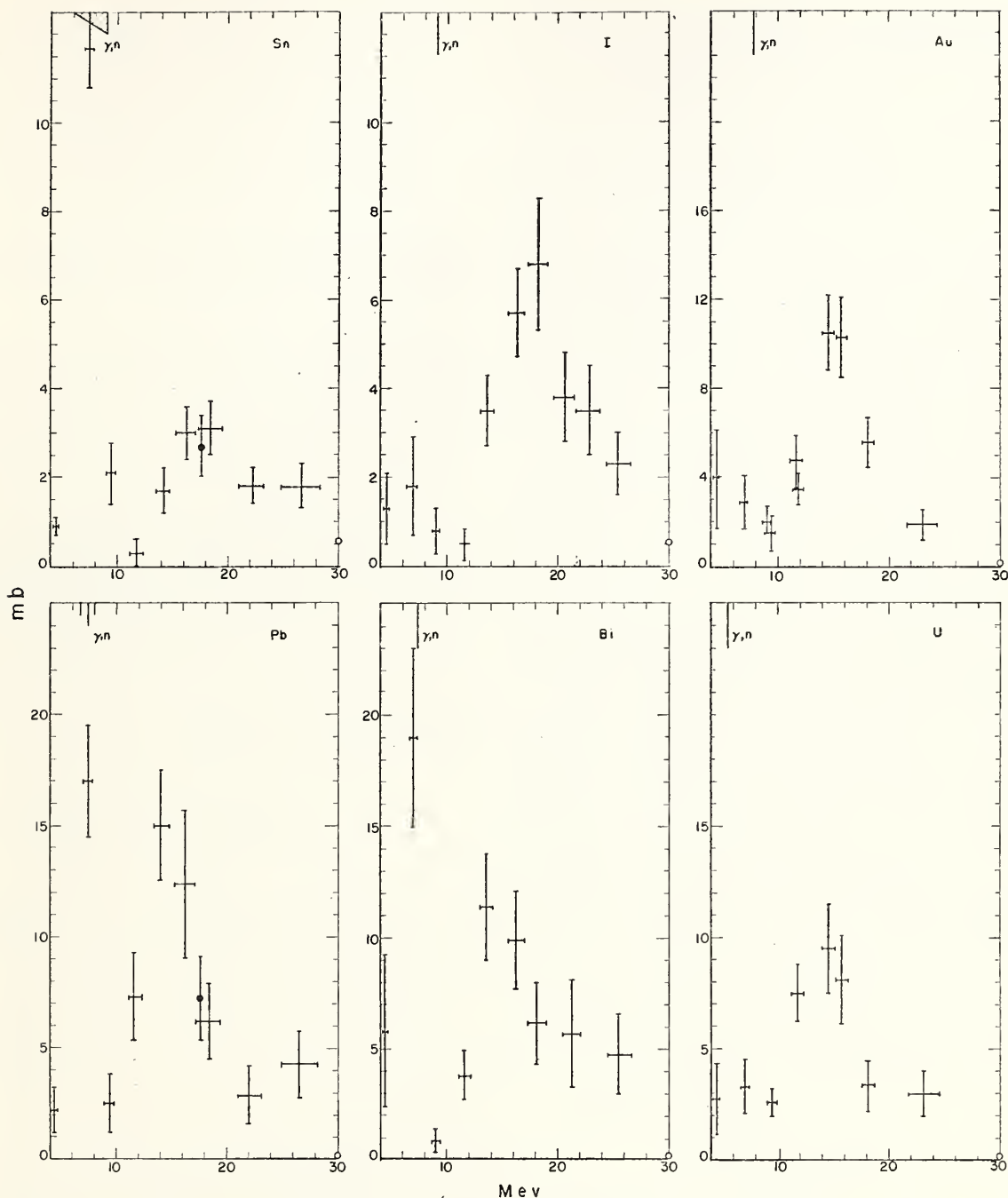


FIG. 6. The elastic scattering cross sections for Sn, I, Au, Pb, Bi, and U. The points at 17.6 Mev are those of Stearns.⁴

distribution as determined from the scattering cross sections is plotted as a function of A in Fig. 7. The line drawn through the points corresponds to the dependence,

$$E_m = 82A^{-1/3}, \quad (7)$$

which is consistent with what is to be expected on the basis of simple hydrodynamical considerations.¹⁴

¹⁴ M. Goldhaber and E. Teller, Phys. Rev. 74, 1046 (1948); H. Steinwedel and J. H. D. Jensen, Z. Naturforsch. 5a, 413 (1950); Ferentz, Gell-Mann, and Pines, Phys. Rev. 92, 836 (1953).

A detailed comparison of the scattering data and the neutron yield data can best be made in terms of the dispersion relation that gives the dependence of the elastic scattering cross section in the forward direction on the total photon absorption cross section.¹⁵ If the transitions involved in the scattering and absorption are dipole, this leads to the following relationship

¹⁵ Gell-Mann, Goldberger, and Thirring, Phys. Rev. 95, 1612 (1954).

between the elastic scattering cross section, $\sigma_s(E)$, and the total absorption cross section, $\sigma_a(E)$:

$$\sigma_s(E) = \frac{1}{6\pi\lambda^2} \left[\sigma_a^2(E) + \left(\frac{2E}{\pi} P \int \frac{\sigma_a(E') dE'}{E'^2 - E^2} \right)^2 \right] + \frac{8\pi}{3} D^2 + \frac{8}{3\pi} \frac{1}{\hbar c} DE^2 P \int \frac{\sigma_a(E') dE'}{E'^2 - E^2}, \quad (8)$$

where D is the Thomson scattering amplitude. The measured scattering cross sections are really averages of the right side of Eq. (8) over an energy band 1 to 2 Mev wide. As long as σ_a is a smooth function of the energy, as it is in the giant resonance region, all of the cross sections appearing in the above expression may be replaced by their average values, since $\langle \sigma_a^2 \rangle_{Av} \simeq \langle \sigma_a \rangle_{Av}^2$. The average scattering cross section can then be calculated from the average absorption cross section. If, on the other hand, the absorption cross section varies rapidly in ΔE , the average scattering cross section will be large compared to that obtained by substituting the average absorption cross section in the dispersion relation.

In order to determine how well the elastic scattering cross section may be predicted from the available photon absorption cross sections, $\sigma_a(E)$ has been calculated by substituting the measured values of $\sigma_a(E)$ for Al and Cu in Eq. (8). The total absorption cross section for Al was taken to be the sum of the (γ, n) and (γ, p) cross sections.^{1,16} The total absorption cross section for Cu was taken as the product of the (γ, n) cross section and the ratio of the integrated total particle yield to the integrated neutron yield given by Byerly and Stephens.¹⁷ The results of these calculations are given by the solid curves in Figs. 4 and 5. It may be seen that $\sigma_s(E)$ for Cu can be predicted satisfactorily from the published photon absorption cross sections. The results for Al indicate that the Al nucleus must absorb photons at considerably higher energies than is implied by the available neutron and proton yield data.

If the absorption cross section, σ_a , has a resonance shape then there is some energy near its peak for which the terms involving the integrals in Eq. (8) vanish and

$$\frac{\sigma_a^2}{\sigma_s - (8\pi/3)D^2} = 6\pi\lambda^2. \quad (9)$$

This expression may be used to compare the elastic scattering data with the neutron yield data at the peak of the giant resonance in order to obtain an indication of how well the total absorption cross section is represented by the (γ, n) cross section. In making this comparison, the nuclear Thomson scattering cross section $(8\pi/3)D^2$, is neglected since it is small compared with the uncertainties in the measured scattering cross

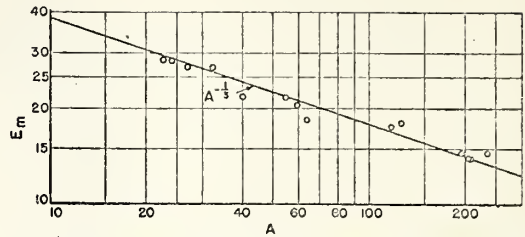


Fig. 7. The dependence of E_m on the atomic mass number A . E_m is the energy of the center of the giant resonance of the scattering curves given in Figs. 4-6. The line drawn through the points corresponds to the dependence $E_m = 82A^{-1/3}$.

sections. The ratio, $\sigma^2(\gamma, n)/\sigma_s$, at the peak of the giant resonance is given in column 2 of Table II for the heavier elements ($A > 50$). This ratio is not given for $A < 50$ because of the large differences in the shapes of the (γ, n) and scattering cross sections and the resultant ambiguities in the meaning of the ratio. Within the errors in the experimental determinations of $\sigma(\gamma, n)$ and σ_s , Eq. 9 is satisfied for all of the heavier nuclei. As is indicated in column 3, better agreement is obtained for Cu and Ni if the ratios given in column 3 are multiplied by the square of the ratio of the neutron plus proton yield cross section to the neutron yield cross section.^{16,17}

Equation (7) may be rearranged and integrated to give

$$6\pi c^2 \hbar^2 \int \frac{\sigma_s(E)}{E^2} dE = \int \sigma_a^2(E) dE + \int dE \left| \frac{2E}{\pi} P \int \frac{\sigma_a(E') dE'}{E'^2 - E^2} \right|^2. \quad (10)$$

In this expression the integral of the Thomson scattering cross section, $(8\pi/3)D^2$, has been neglected because this cross section is small compared to any of the measured scattering cross sections. The last term in Eq. (8) is also omitted since contributions from either side of the giant resonance tend to cancel in the integration. In the case of Al and Cu the integral of this term was less than 10% of the two remaining terms in Eq. (8).

Both sides of Eq. (10) have been crudely evaluated using the scattering cross sections measured in the present experiment and the published neutron yield cross sections^{1,2} for the same elements. The integrations were done only over the giant resonances, i.e., from the (γ, n) threshold to 25 Mev for $A > 50$ and to 40 Mev for $A < 50$. The contribution from the sometimes large scattering cross section below the threshold was omitted since it results from the absorption by lines having widths small compared to their spacing and for which the substitution of $\langle \sigma_a \rangle_{Av}^2$ for $\langle \sigma_a^2 \rangle_{Av}$ is not valid.

The results of these integrations divided by $(NZ/A)^2$ are compared in Fig. 8. Since $\int \sigma_a dE = 0.06NZ/A \times (1 + 0.8x)$, the integrals of Eq. (10) should be roughly proportional to $(NZ/A)^2$ and the points of Fig. 8 should

¹⁶ J. Halpern and A. K. Mann, Phys. Rev. 83, 370 (1951).

¹⁷ P. Byerly and W. E. Stephens, Phys. Rev. 83, 54 (1951).

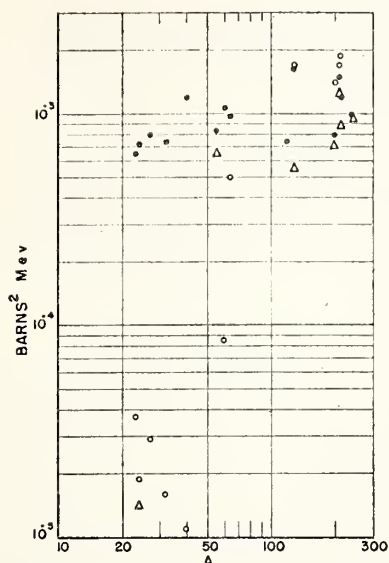


FIG. 8. A plot of the integrals of Eq. (10) as a function of A . The dots are the left side of Eq. (10) divided by $(NZ/A)^2$ obtained from the data of the present experiment. The open circles and triangles are the right side of Eq. (10) divided by $(NZ/A)^2$ obtained from the neutron yield data of references 1 and 2, respectively.

lie on a horizontal line the height of which is determined by the sum rule.¹⁸ The points obtained from the scattering data are all consistent with those obtained from the neutron yield data for the heavy elements for which the integrated neutron yield cross sections are known to exhaust the dipole sum.

The values of the scattering integrals for the low- Z nuclei extrapolate smoothly from the values obtained for the heavier nuclei. This is in contrast to the results obtained for the integrals of the neutron yield cross sections where the values fall off markedly below $A = 50$. The high values of the scattering integrals for Na, Mg, Al, S, and Ni can, of course, be explained by assuming that all of the photon absorption for these nuclei is due to sharp, well-defined levels. It would be a remarkable coincidence, however, if the strengths and distributions of the levels in these five nuclei would have just the right values for the scattering integrals to fall on a smooth extrapolation of the values obtained for the heavier nuclei. A more reasonable explanation would be that the absorption cross section for these nuclei is made up principally of a smooth slowly varying function of the energy. These data then indicate that the (γ, n) cross section represents only a fraction of the total absorption cross section.

The integrals evaluated from the neutron yield data can be corrected to include proton emission by multiplying them by the square of the ratio of the neutron plus proton yield to the neutron yield.^{1,2,16,19} This raises the points for Mg to 2.7×10^{-4} and 2.0×10^{-4} barns² Mev, and the points for Al, S, Ca, and Ni to 1.2 , 4.9 , 6.6 , and 3.4×10^{-4} barns² Mev, respectively. After correction for the proton yields the absorption integrals for Mg, Al, and Ni are still below the scattering integrals by a factor of approximately three. The integrals for S and Ca are in agreement with the scattering integrals. It should be pointed out that for Al and Ni the corrections were made using the actual (γ, n) and (γ, p) cross sections as a function of energy.^{1,16} For Mg, S, and Ca the corrections involve the use of data obtained from the ratio of the proton yields produced by a 28-Mev bremsstrahlung spectrum to that produced by a 23.5-Mev bremsstrahlung spectrum.¹⁹ The agreement of the integrals (S and Ca) calculated from the scattering data and the absorption data corrected for proton emission may be fortuitous in view of the fact that the absorption cross sections used in calculating the integrals both peaked below 22 Mev while the scattering data indicate that there is considerable absorption at energies above 24 Mev.

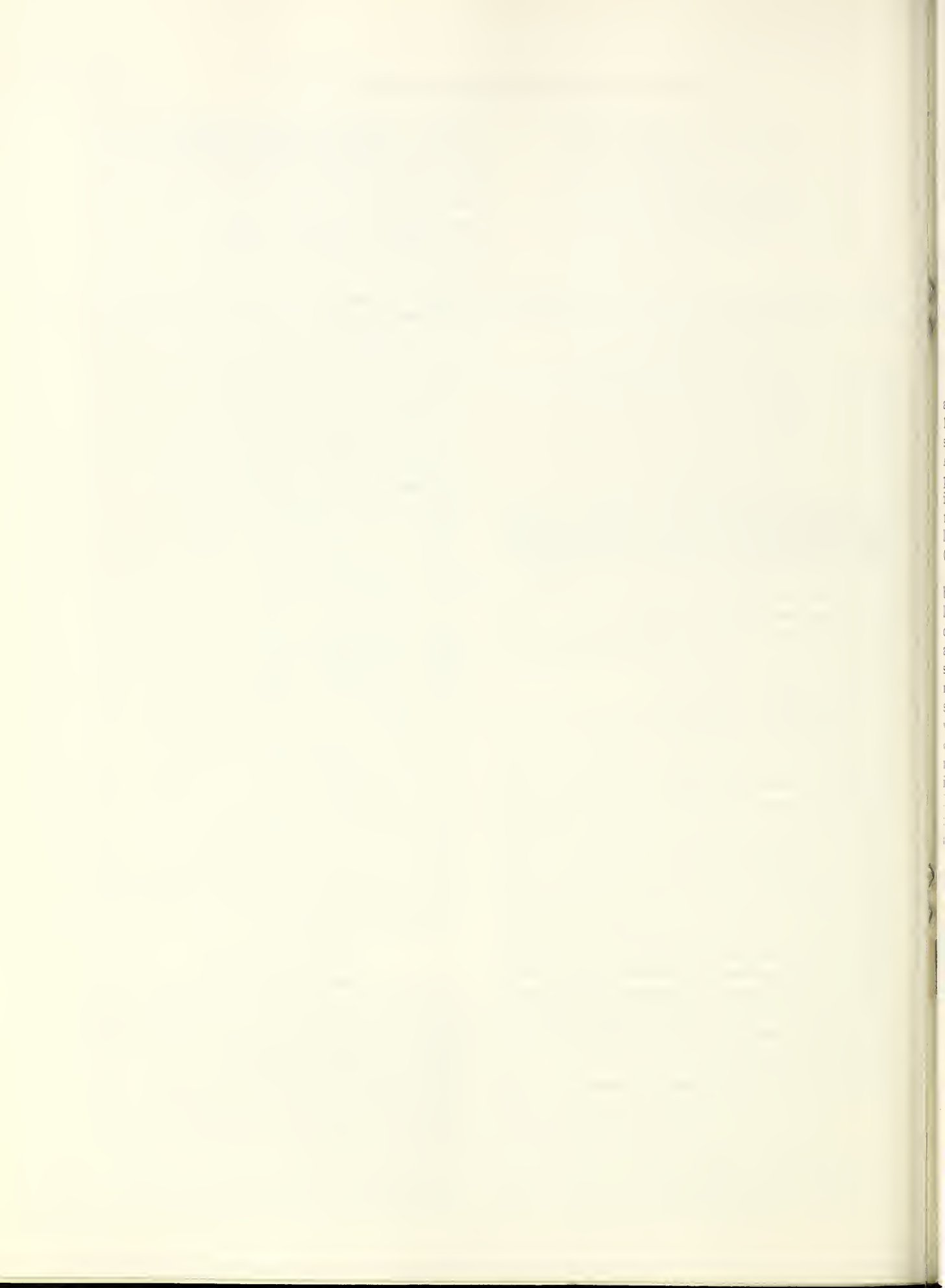
In conclusion, the data of this experiment indicate that both the scattering integral and the energy corresponding to the center of the oscillator strength distribution vary rather smoothly from Na to U. This is in contrast with the data obtained from the neutron yield experiments where both the integrated cross sections and the energies of the maxima in the yield curves start to fall below the values predicted by the sum rule and simple hydrodynamical considerations for nuclei less than about $A = 50$. The scattering data indicate that the giant resonance for the light nuclei is both considerably broader and centered at a higher energy than the presently available data on the (γ, p) and (γ, n) reactions would imply. In this connection it should be pointed out that no extensive measurements of the particle yield cross sections have been made at energies greater than 24 Mev.

ACKNOWLEDGMENTS

The authors thank Dr. U. Fano and Dr. H. W. Koch for their continued interest and support, and N. Svantesson for his collaboration in some of the latter phases of the work. Special thanks go to Dr. M. Danos for many very fruitful discussions.

¹⁸ J. S. Levinger and H. A. Bethe, Phys. Rev. 78, 115 (1950).

¹⁹ S. A. E. Johansson, Phys. Rev. 97, 1186 (1955).



Photon Self-Absorption and Scattering by the 15.1-Mev Level in C^{12} †

EVANS HAYWARD AND E. G. FULLER
National Bureau of Standards, Washington, D. C.

(Received February 19, 1957)

Bremsstrahlung x-rays have been used to excite the 15.1-Mev level in C^{12} . The integral scattering cross section of 19.0 ± 0.27 Mev mb has been determined by measuring the absolute number by 15.1-Mev x-rays scattered. The peak absorption cross section 22.2 ± 2.2 barns has been obtained from a self-absorption experiment. These results combine to give 54.5 ± 9.3 ev for the ground state radiation width and 79 ± 16 ev for the total width of the level.

INTRODUCTION

A NUMBER of particle reactions¹ have been used to excite a 15.1-Mev level in C^{12} . This level has also been excited by irradiating a carbon target with 15.1-Mev x-rays.² The angular distribution of the scattered x-rays is consistent with dipole scattering.³ Although this level is well above the threshold for alpha-particle decay, Kavanagh⁴ has found $\Gamma_\alpha/\Gamma_\gamma < 0.5$. The inhibited alpha-particle decay and the dipole nature of the ground-state transition establish this level as belonging to the $T=1, J=1+$ isobaric spin triad B^{12}, C^{12}, N^{12} .

This paper is an account of an experiment in which bremsstrahlung x-rays have been used to study this level. It contains a description of the methods used to determine the peak absorption cross section in the level and the integral scattering cross section. The peak absorption cross section was determined from a measurement of the attenuation of the 15.1-Mev photons scattered by a carbon target when a carbon absorber was placed in the incident beam. The integral scattering cross section was obtained by measuring the absolute number of 15.1-Mev photons scattered by a target irradiated in a bremsstrahlung beam of known intensity. From these two quantities the branching ratio corresponding to ground-state radiative transitions, Γ_γ/Γ , and the ground-state radiation width, Γ_γ , were obtained.

EXPERIMENTAL ARRANGEMENT

Except for some improvements in the shielding around both the betatron and the detector, the experimental arrangement was the same as the one used in a previous experiment.⁵ The arrangement is shown in Fig. 1.

† This research was supported by the U. S. Air Force, through the Office of Scientific Research of the Air Research and Development Command.

¹ V. R. Johnson, Phys. Rev. 86, 302 (1952); Cohen, Moyer, Shaw, and Waddell, Phys. Rev. 96, 714 (1954); Rasmussen, Ree, Sampson, and Wall, Phys. Rev. 96, 812 (1954); Bigham, Allen, and Almqvist, Phys. Rev. 99, 631 (1955); C. A. Barns and R. W. Kavanagh, Phys. Rev. 100, 1796 (1955).

² Fuller, Hayward, and Svantesson, Bull. Am. Phys. Soc. Ser. II, 1, 21 (1956); E. Hayward and E. G. Fuller, Physica, 22, 1138 (1956).

³ J. E. Leiss and J. M. Wyckoff, Bull. Am. Phys. Soc. Ser. II, 1, 197 (1956).

⁴ R. W. Kavanagh, Ph.D. dissertation, California Institute of Technology, 1956 (unpublished).

⁵ E. G. Fuller and Evans Hayward, Phys. Rev. 101, 692 (1956).

The important modifications were: (1) a twenty-channel pulse-height analyzer was used to take the data, (2) the solid angle of the detector was no longer defined by the dimensions of the NaI(Tl) crystal but by a 3-inch diameter hole through a 5-inch lead plug placed in front of it, (3) the Lucite absorber placed between the target and detector to remove electrons and low-energy photons emitted by the target was made as thin as possible ($4-8$ g/cm²) to minimize the degradation of the scattered photons.

The pulse-height distribution obtained when a 19-Mev bremsstrahlung beam filtered by 97 g/cm² of aluminum irradiates a 1.98 g/cm² polystyrene target is given by the histogram in Fig. 2. As will be shown later, the sharp rise in the pulse spectrum below nine millivolts pulse height is not associated with the 15.1-Mev line and probably results from multiple processes in the target. Based on an extrapolation from the 1.13-Mev line from a Zn⁶⁵ source, the peak in this pulse-height distribution corresponds to a photon energy near 15 Mev. The threshold for the production of the carbon line is 15.0 ± 0.2 Mev. This threshold is based on the energy scale for the betatron determined by observing the (γ, n) thresholds in Be⁹, B¹⁰, Cu⁶³, and Cu⁶⁵.

The two experiments described below were performed by using graphite and polystyrene targets and absorbers approximately 2 g/cm² thick. A bremsstrahlung energy of 19 Mev was chosen in order to maximize the number of 15.1-Mev photons scattered without introducing appreciable neutron background from the $C^{12}(\gamma, n)C^{11}$ process and to eliminate the possibility of feeding the 15-Mev state from higher levels.

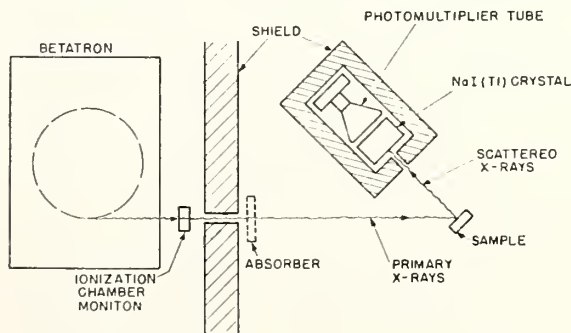


FIG. 1. The experimental arrangement.

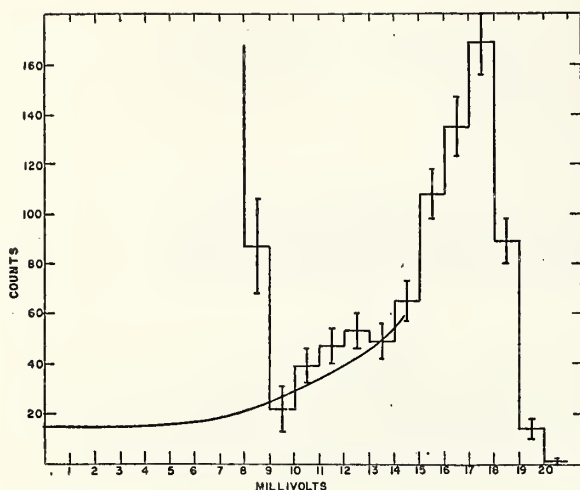


FIG. 2. The pulse-height distribution produced in the NaI(Tl) crystal when a 1.98-g/cm² polystyrene target was irradiated by a 19-Mev bremsstrahlung beam filtered through 97 g/cm² of Al. The solid line represents the extrapolation used to obtain the total number of interactions produced in the crystal by 15.1-Mev photons.

All runs were monitored in terms of the charge produced in the transmission ionization chamber indicated in Fig. 1. This charge was collected on a polystyrene film condenser, the voltage across which was measured with an Applied Physics Corporation Model 30 Vibrating Reed Electrometer.

THE SELF-ABSORPTION EXPERIMENT

The self-absorption experiment from which the peak absorption cross section in the level was obtained was a relative measurement. It consisted of observing the attenuation of the scattered photons when an absorber of the target material was placed in the incident beam. These data were taken in a series of runs made alternately with and without the absorber. Each run lasted approximately 40 minutes. In the "absorber out" runs approximately 150 counts were obtained in each run in the 10 to 20 mv region of the pulse-height distribution shown in Fig. 2. All runs taken under the same conditions were consistent with each other within the statistical uncertainties of the data.

In addition the attenuation produced by an aluminum absorber placed in the incident beam as well as that produced by carbon and aluminum absorbers placed in the scattered beam was measured. The results of the attenuation measurements are given in Table I.

TABLE I. Attenuation measurements.

Thickness g/cm ²	Absorber	$I(\Delta)/I(0)$	$e^{-\sigma_n \Delta}$
2.07	C in incident beam	0.511 ± 0.025	0.97
1.62	Al in incident beam	1.1 ± 0.1	0.97
13.7	Al in scattered beam	0.64 ± 0.05	0.74
7.77	C in scattered beam	0.81 ± 0.07	0.87

The attenuations are compared with those to be expected from electronic absorption alone. The fact that self-absorption was observed when the carbon absorber was placed in the incident beam and not observed when the absorber was in the scattered beam indicates that the level width is small compared to the energy given to the recoiling carbon nucleus. At 120° this energy is about 30 kev.

Quantitatively it follows from Eq. (5) of reference 5 that the number of photons scattered by a target of thickness T , in which the nuclear scattering cross section is $\sigma_s(E)$ and the nuclear and electronic absorption cross sections are, respectively, $\sigma_n(E)$ and σ_e , is proportional to:

$$Y(0) = \int dE \frac{\sigma_s(E)}{1 + \sigma_n(E)/2\sigma_e} \times [1 - e^{-(\sigma_n(E) + 2\sigma_e)NT / \cos\theta}]. \quad (1)$$

The number of pulses registered in the nine channels around the peak of the distribution of Fig. 2 have been taken as a measure of $Y(0)$. Similarly the number of pulses observed in this peak when an absorber of thick-

TABLE II. Target and absorber properties.

	Graphite	Polystyrene
Target	2.07 g/cm ²	1.98 g/cm ²
Absorber	2.07 g/cm ²	1.98 g/cm ²
$2\sigma_e$	0.674 b	0.758 b
$I(\Delta)/I(0)$	0.529 ± 0.026	0.543 ± 0.017

ness Δ is placed in the incident beam is proportional to:

$$Y(\Delta) = e^{-\sigma_e \Delta} \int dE \frac{e^{-\sigma_n \Delta} \sigma_s(E)}{1 + \sigma_n(E)/2\sigma_e} \times [1 - e^{-(\sigma_n + 2\sigma_e)NT / \cos\theta}]. \quad (2)$$

The ratio

$$Y(\Delta)/Y(0) = e^{-\sigma_e \Delta} I(\Delta)/I(0) \quad (3)$$

has been determined experimentally. The ratios $I(\Delta)/I(0)$ calculated from the experimental results are shown in Table II along with the properties of the targets and absorbers.

The ratio $I(\Delta)/I(0)$ may be evaluated by numerical integration for comparison with the experiment. It depends on the shape of $\sigma_n(E)$ as a function of the energy and on its maximum value, σ_n^0 . In the absence of thermal Doppler broadening, $\sigma_n(E)$ for a single level is given by a Breit-Wigner expression:

$$\sigma_n(x) = \sigma_n^0 / (1 + x^2), \quad (4)$$

where $x = (E - E_0) / (\frac{1}{2}\Gamma)$. The curve labelled $t=0$ in Fig. 3 is a plot of $I(\Delta)/I(0)$ as a function of σ_n^0 . This curve was calculated numerically for the polystyrene absorber and target used.

In general the absorption cross section is distorted owing to the thermal motions of the target nuclei. The resonance is effectively widened and its peak depressed by an amount proportional to the ratio of the Doppler width, δ , to the level width, Γ . The Doppler-broadened Breit-Wigner cross section obtained by combining the single-resonance formula with a Gaussian of width δ is⁶:

$$\sigma_n(x,t) = \sigma_n^0 \frac{1}{2(\pi t)^{1/2}} \int \frac{\exp[-(x-y)^2/4t]}{1+y^2} dy, \quad (5)$$

where $t = (\delta/\Gamma)^2$. This function is available in tabular form⁷ and has been inserted into the integrals of Eq. (3) to obtain the ratios, $I(\Delta)/I(0)$, plotted in Fig. 3 for three values of the parameter t .

The horizontal lines in Fig. 3 represent the most probable value and the limit of error of the observed ratio $I(\Delta)/I(0)$. For values of t between 0 and 1 the observed attenuation is consistent with a peak absorption cross section of about 24 barns. A similar set of curves calculated for the parameters corresponding to the graphite target and absorber gave similar results. It will be shown later that values of $t > 1$ do not give results consistent with both the self-absorption and scattering experiments.

INTEGRAL SCATTERING CROSS SECTION

The scattering cross section for a single level cannot be determined by the method used in the elastic scattering experiment.⁵ This is because the spectrum of

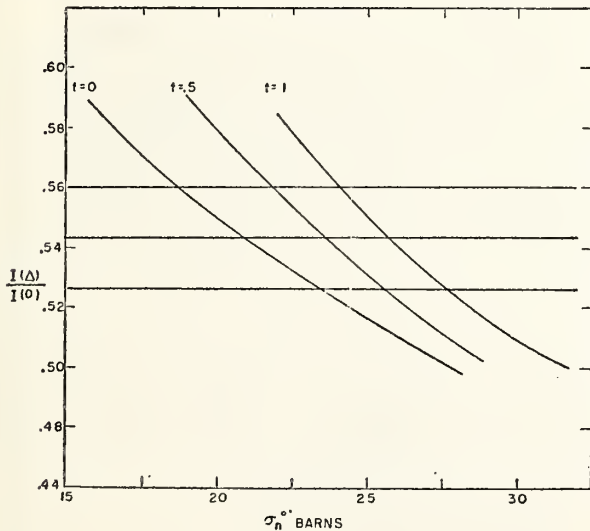


FIG. 3. The smooth curves represent the ratio of the integrals $I(\Delta)/I(0)$ as a function of the peak absorption cross section in the levels for three values of the parameter $t = (\delta/\Gamma)^2$. The horizontal lines represent the most probable value and limits of error obtained for this ratio from the observed transmission.

⁶ H. A. Bethe, Revs. Modern Phys. 9, 71 (1937), Sec. 61.

⁷ Rose, Miranker, Leak, Rosenthal, and Hendrickson, Westinghouse Atomic Power Division Report SR-506, 1954 (unpublished), Vols. I and II.

scattered photons, consisting of a sharp well-defined line, is very different from the incident continuous bremsstrahlung spectrum.

From Eq. (5) of reference 5 it can readily be shown that the number of photons scattered will be given by⁸:

$$C = \frac{\Delta\Omega}{13.3} \frac{n(15)}{2\sigma_e} \int dE \frac{\sigma_n(E)}{1 + \sigma_n(E)/2\sigma_e} [1 - e^{-(\sigma_n + 2\sigma_e)NT / \cos\beta}] = \frac{\Delta\Omega}{13.3} \frac{n(15)}{2\sigma_e} I(0). \quad (6)$$

In this expression $\Delta\Omega$ is the solid angle for detecting a photon scattered at 120° ; the number 13.3 is the ratio of the total cross section to the differential cross section at 120° for an angular distribution of the scattered radiation varying as $(1 + \cos^2\theta)$; $n(15)$ is the number of 15.1-Mev photons per Mev incident on the scattering target. The determination of the scattering integral then required the absolute measurement of C , $n(15)$, and $\Delta\Omega$.

The solid angle, $\Delta\Omega$, was taken to be the geometrical solid angle for a photon scattered by a point at the center of the beam on the front surface of the target. This solid angle was 0.0344 steradian. The use of this figure was justified by two experiments. A small radioactive source scanned across the surface of the target showed that to within the statistical accuracy of the measurements ($\pm 2\%$) the average solid angle over the target area was equal to the solid angle for detecting a photon scattered at its center. It was also shown with a standard Co^{60} source that this solid angle is within 5% the geometrical solid angle.

The number of 15.1-Mev photons scattered into $\Delta\Omega$ is the number of interactions they produce in the crystal divided by the detection efficiency. The efficiency is the product of the fraction of the photons that are not removed by the Lucite absorber of thickness D , $e^{-\mu D}$, and the probability that an interaction does take place in the NaI(Tl) crystal of length Z , $1 - \exp(-\mu_{\text{NaI}} Z)$. The attenuation of the scattered 15.1-Mev photons was measured as a function of the thickness of Lucite placed in the scattered beam. These data showed that no appreciable error was made by using the narrow beam absorption coefficient in calculating the number of photons that pass through the Lucite absorber.

The number of interactions in the crystal produced by 15.1-Mev photons was determined from the pulse-height distribution shown in Fig. 2. When a carbon absorber was placed in the incident beam the pulses larger than nine mv were attenuated in the same way as those in the peak of the distribution and are therefore associated with the 15.1-Mev line. The large number of smaller pulses were not absorbed in the appropriate way and must result from multiple processes in the target. The solid line in Fig. 2 represents the extrapolation used to

⁸ The $\cos\beta$ factor in the denominator of Eq. (5) of reference 5 is in error. The cross sections given there are 13% too high.

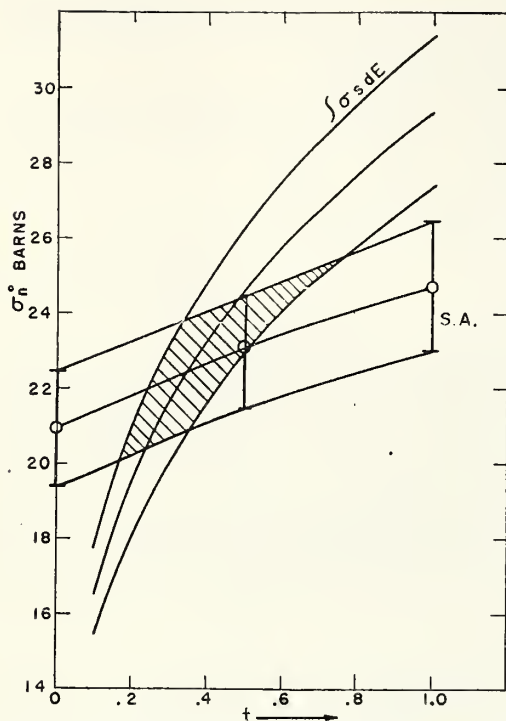


Fig. 4. The peak absorption cross section, σ_n^0 , as a function of t as derived from the two experiments. The points at $t=0, 0.5$, and 1 have been read from the curves of Fig. 3. The smooth curves are plots as a function of t of the expression:

$$\sigma_n^0 = \left[\frac{2}{\pi} \frac{\sqrt{t}}{\delta} 6\pi\lambda^2 \int \sigma_s dE \right]^2.$$

The experimental value of the integral scattering cross section and its limits of error have been used to obtain the three curves. The cross-hatched area is that consistent with both the integral scattering cross section and the self-absorption measurements.

obtain the total number of interactions. The slight rise in the pulse-height distribution near 12 mv represents not more than ten percent of the scattered photons. It probably results from 12.8- and 10.7-Mev photons produced in elastic scattering by the 12.8-Mev level⁹ and inelastic transitions from the 15.1- to the 4.43-Mev level in C^{12} . The extrapolation has been made to exclude this contribution and the integral scattering cross section obtained therefore corresponds only to elastic scattering events.

The determination of $n(15)$ was made by calibrating the transmission ionization chamber used to monitor the exposure in terms of the absolute response of a 25-r Victoreen thimble chamber in an $\frac{1}{8}$ -in. Pb cap.¹⁰ The number of photons per Mev at 15 Mev was obtained

⁹ Gove, Litherfield, and Almqvist, *Bull. Am. Phys. Soc. Ser. II*, 2, 51 (1957); C. N. Waddell (private communication).

¹⁰ *National Bureau of Standards Handbook 55* (U. S. Government Printing Office, Washington, D. C. 1954). This calculated response has been checked experimentally to within 5% at 22 Mev calorimetrically [Laughlin, Beattie, Henderson, and Harvey, *Am. J. Roentgenol. Radium Therapy, Nuclear Med.* 70, 294 (1953)], and at 19 Mev by E. G. Fuller (unpublished data) using the total spectrum method [Koch, Leiss, and Pruitt, *Bull. Am. Phys. Soc. Ser. II*, 1, 199, (1956)].

from the 19-Mev Schiff spectrum as tabulated by Penfold and Leiss¹¹ after normalizing this spectrum to the intensity used in the scattering runs and correcting for the attenuation in the 97 g/cm² of aluminum filter used in the incident bremsstrahlung beam.

From Eq. (6), since $\sigma_e \ll \sigma_n$, it can be seen that if $\sigma_n(E)$ is the same function of energy for polystyrene and graphite, then the product $N\sigma_e$ will be constant when one target is substituted for the other. The product $N\sigma_e$ was found experimentally to be the same within $\pm 3\%$. This result implies either that the Doppler width is the same for the two materials or that it is small compared to the level width, Γ .

Combining the measured quantities for polystyrene and graphite gives $(9.5 \pm 1.3) \times 10^{-5}$ Mev-b for the scattering integral, $I(0)$. The quoted error results from counting statistics $\pm 3\%$, monitor calibration $\pm 8\%$, determination of the solid angle $\pm 5\%$, and extrapolation of the pulse-height distribution $\pm 10\%$.

The quantity which is of interest theoretically is not the experimentally determined scattering integral $I(0)$, but the actual integral scattering cross section, $\int \sigma_s(E) dE$. The ratio, R , of $\int \sigma_s(E) dE$ to $I(0)$ depends both on the size of the nuclear absorption cross section and on its energy dependence. This ratio has been evaluated for the three values of t used in the analysis of the self-absorption experiment and for the corresponding values of σ_n^0 derived from the observed attenuation. The values obtained center around $R=20$ and vary by only 3% over the range of t considered so that $\int \sigma_s(E) dE = 1.90 \pm 0.27$ Mev-mb.

ANALYSIS OF THE DATA AND DISCUSSION

The value of the peak absorption cross section derived from the experimental data as presented in Fig. 3 depends on the value of the parameter t assumed. The range of values of σ_n^0 and t consistent with both the self-absorption and scattering experiments were found in the following way: Values for the peak absorption cross section, σ_n^0 , consistent with the self-absorption experiment have been read from the curves of Fig. 3 for the three values of t given in Fig. 3. Similar values were obtained from the graphite data. For each value of t the value of σ_n^0 obtained from the polystyrene and graphite data agreed well within the experimental errors. The two sets of data were then averaged to obtain a value for the peak absorption cross section at each value of t . These points are shown in Fig. 4.

The integral scattering cross section may also be expressed in terms of σ_n^0 and t :

$$\int \sigma_s(E) dE = \frac{\pi}{2} \frac{\Gamma_\gamma}{1} \sigma_n^0 = \frac{\pi}{2} \frac{\delta}{\sqrt{t}} \frac{(\sigma_n^0)^2}{6\pi\lambda^2}, \quad (7)$$

since $\Gamma_\gamma/1 = \sigma_n^0/6\pi\lambda^2$ for a dipole transition. The smooth

¹¹ A. S. Penfold and J. E. Leiss, *Phys. Rev.* 95, 637 (1954).

curves in Fig. 4 are a plot of σ_n^0 versus t where the experimental value of $\int \sigma_n dE$ and its limits of error have been used to obtain the three curves.¹² The cross-hatched area is that consistent with the two experiments.

The best value of the peak absorption cross section consistent with both experiments is 22.2 ± 2.2 barns. This result was obtained from Fig. 4. The branching ratio is then: $\Gamma_\gamma/\Gamma = \sigma_n^0/\sigma\pi\lambda^2 = 22.2/32 = 0.69 \pm 0.07$. The ground state radiation width, Γ_γ , may be obtained from Eq. (7) by combining σ_n^0 with the measured value for the integral scattering cross section. The result, $\Gamma_\gamma = 54.5 \pm 9.3$ ev, may be compared to the single-

¹² In calculating σ_n^0 from this expression a value for δ of 45 electron volts was assumed. This is the value of the Doppler width given by the mean energy of the carbon nuclei in the diamond lattice. The mean energy was calculated from the frequencies of the diamond lattice given by H. M. J. Smith [Trans. Roy. Soc. (London) 241, 105, (1948)]. The value of the Doppler width obtained in this way is probably an upper limit. A lower limit would be 31.6 electron volts; the value corresponding to a gas of carbon atoms at room temperature. The upper limit was used since in the targets used the mean energy of the carbon nuclei will be determined chiefly by the presence of the carbon-carbon bond [E. Montroll (private communication)]. Fortunately, the value of σ_n^0 derived from a plot such as given in Fig. 4 is not sensitive to the exact value assumed for δ .

TABLE III. Properties of the 15.1 Mev, $T=1$, $J=1+$ level in C^{12} .

Radiation width to the ground state of C^{12}	54.5 ± 9.3 ev
Total level width	79 ± 16 ev
Radiation width to the 4.43-Mev state of C^{12}	$\leq 5.5 \pm 0.9$ ev
Alpha particle width to the 2.9-Mev state of Be^8	$(18.6 \leq \Gamma_\alpha \leq 24.5) \pm 8.2$ ev

particle radiation width of 65 ev given by Moszkowski.¹³

The 15.1-Mev level in C^{12} also decays by gamma-ray emission to the 4.43-Mev state in C^{12} and by α -particle emission to the $J=2^+$ state in Be^8 . (Decay to the 0^+ ground state of Be^8 is forbidden.) From the pulse-height distribution of Fig. 2 an upper limit of ten percent may be placed on the branching ratio to the 4.43-Mev level, $\Gamma_{4.43}/\Gamma_\gamma \leq 0.1$. If one assumes no transitions to the 4.43-Mev state in C^{12} , these data give as an upper limit for alpha-particle decay, $\Gamma_\alpha/\Gamma_\gamma \leq 0.45 \pm 0.15$. This result is consistent with the upper limit of 0.5 given by Kavanagh.⁴ The properties of the 15.1-Mev level in C^{12} obtained from this experiment are summarized in Table III.

¹³ S. A. Moszkowski, *Beta- and Gamma-Ray Spectroscopy*, edited by Kai Siegbahn (Interscience Publishers, Inc., New York, 1955), p. 373.



Shape of the High-Energy End of the Electron-Bremsstrahlung Spectrum*

E. G. FULLER, E. HAYWARD, AND H. W. KOCH
National Bureau of Standards, Washington, D. C.

(Received October 9, 1957)

The elastic scattering of photons by the 15.11-Mev level in C^{12} has been used to study with good energy resolution the number of photons at the high-energy end of a bremsstrahlung spectrum. The bremsstrahlung was produced by electrons accelerated in a betatron, the energy of which was varied in 35-kev increments. Targets were: a 0.025-inch-diameter tungsten wire and the following foils, 0.001- and 0.010-inch tungsten, 0.002-inch thorium and 0.010-inch nickel. The foils were used to study the dependence of the spectrum shape upon target thickness and atomic number. When compared with Bethe-Heitler spectra corrected for target thicknesses, the data indicate an excess number of photons in the tip of the spectrum. The experimental number depends on the atomic number of the target and cannot vary more rapidly than Z^4 .

I. INTRODUCTION

THERE have been a number of experimental measurements of the bremsstrahlung spectra generated by electrons having energies in the range from 1 to 20 Mev. A review of these experiments and the comparison of the experiments with the available theories is given by Starfelt and Koch.¹ The data indicate that for high energies the general shape of the bremsstrahlung spectrum is well described by the results obtained from a calculation made in Born approximation when the effect of screening by the atomic electrons is taken into account.² The absolute magnitudes of the brems-

strahlung cross section for electrons with energies in the 10- to 20-Mev range have been found to agree with the Born approximation result to within about 10%.^{1,3}

Up to the present time there have been no detailed measurements or satisfactory theoretical calculations of the shape of the high-energy tip of the bremsstrahlung spectrum (energies within mc^2 of the incident electron kinetic energy). The shape of the spectrum in this energy range is of utmost importance in interpreting the breaks that have been found in activation curves.⁴ Poor instrumental resolution has been the principal reason for the lack of experimental information about this portion of the bremsstrahlung spectrum. The failure to obtain a satisfactory theoretical prediction for the shape of the tip of the spectrum can be laid to

* This work was partially supported by the U. S. Air Force, through the Office of Scientific Research of the Air Research and Development Command.

¹ N. Starfelt and H. W. Koch, *Phys. Rev.* **102**, 1598 (1956).

² H. A. Bethe and W. Heitler, *Proc. Roy. Soc. (London)* **A146**, 83 (1934).

³ E. V. Weinstock and J. Halpern, *Phys. Rev.* **100**, 1293 (1955).

⁴ A. S. Penfold and B. M. Spicer, *Phys. Rev.* **100**, 1377 (1955).

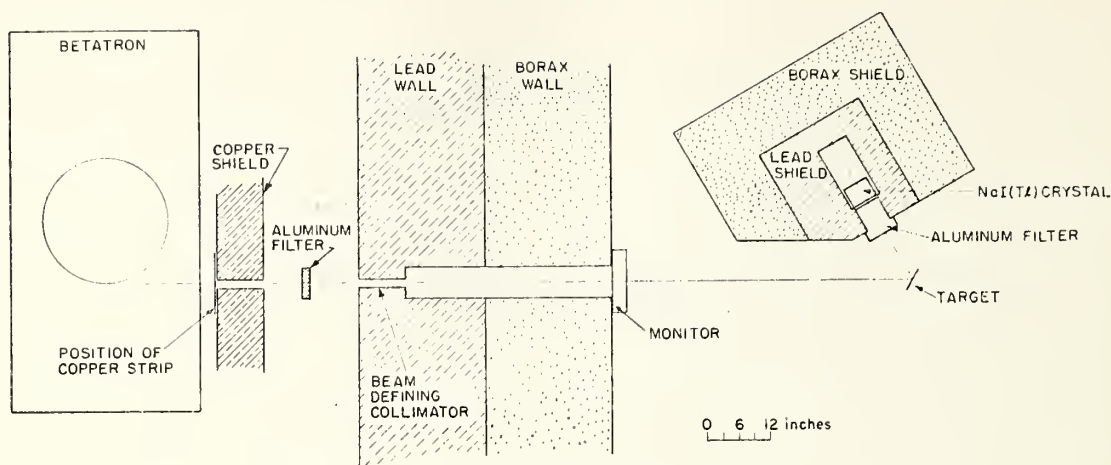


FIG. 1. The experimental arrangement.

the extreme difficulties encountered when calculations must be made using the exact wave functions to describe the incoming and outgoing electron.

The technique of studying the shape of the bremsstrahlung spectrum by use of the photoexcitation of nuclear energy levels has been shown to be possible at low energies⁵ and in the 10- to 20-Mev range.^{4,6} This paper will describe an experiment in which this technique was employed. In addition to the spectrum from a 0.025-inch tungsten wire target, which is normally used in the National Bureau of Standards betatron, spectra were also measured from 0.010-inch nickel, 0.001-inch tungsten, 0.010-inch tungsten, and 0.002-inch thorium foil targets placed inside the accelerating tube. The results for the shape of the high-energy tip of the spectrum are compared in this paper with spectra calculated from the Born approximation result given by Bethe and Heitler.⁷

II. EXPERIMENTAL METHOD

In this experiment the shape of the bremsstrahlung spectrum was studied by observing the scattering by the 15.11-Mev level in C^{12} as a function of the maximum energy of the betatron. In the laboratory system the threshold for scattering by this level is 15.12 Mev. The width of this level has been shown to be 79 ± 16 ev.⁸ The number of photons scattered is then a measure of the number of photons in a very narrow energy band of the bremsstrahlung spectrum. For this work the yield curve is defined as the curve giving the relative number of 15.12-Mev photons per Mev in the total bremsstrahlung spectrum as a function of the peak energy of the spectrum. The object of the experiment was to study the shape of the yield curve for various

types of bremsstrahlung targets placed inside the betatron donut.

The experimental arrangement used is shown in Fig. 1. The counting rate for the photons scattered by the 15.11-Mev level was optimized by placing as much aluminum absorber as space would allow in the scattered beam. This procedure had the effect of decreasing the counting rate resulting from low-energy photons and electrons relative to that resulting from the high-energy photons. The absorber in the primary beam was then adjusted until it was possible to run with full output from the betatron at 16 Mev without having appreciable pile-up in the peak of the pulse-height distribution produced by the photons scattered by the 15.11-Mev level. The pulse-height distribution produced by the photons scattered from a 2-g/cm² graphite target is shown in Fig. 2. The pulses between *A* and *B* on this distribution were used as a measure of the

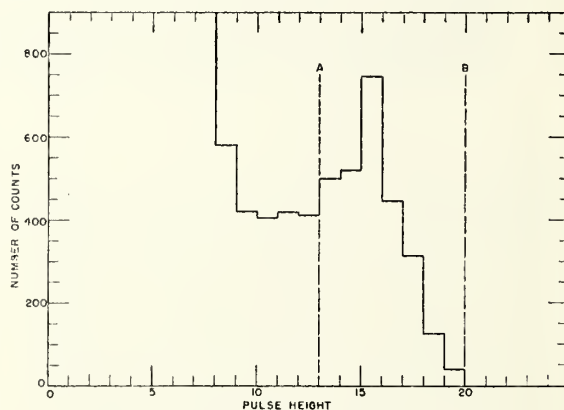


FIG. 2. The pulse-height distribution obtained when the carbon target was irradiated by 16- to 17-Mev bremsstrahlung beams. The number of counts between *A* and *B* were taken as a measure of the number of 15.12-Mev photons in the bremsstrahlung beam. This distribution contains relatively many more small pulses than the one shown in reference 8 because of the degradation of the scattered photons in the large aluminum filter used in the present experiment.

⁵ W. C. Miller and B. Waldman, *Phys. Rev.* **75**, 425 (1949).

⁶ Fuller, Hayward, and Svantesson, *Bull. Am. Phys. Soc. Ser. II*, **1**, 10 (1956); Sargent, Bertozzi, and Demos, *Bull. Am. Phys. Soc. Ser. II*, **1**, 343 (1956).

⁷ W. Heitler, *Quantum Theory of Radiation* (Oxford University Press, New York, 1954), third edition, Eq. (16), p. 245.

⁸ E. Hayward and E. G. Fuller, *Phys. Rev.* **106**, 991 (1957).

number of 15.12-Mev photons in the incident spectrum. At 19 Mev the counting rate was approximately 200 counts per hour in this region of the pulse-height distribution.

When data were obtained for bremsstrahlung spectra with operating energies greater than 20 Mev, there was some evidence that counts in the region from *A* to *B* were produced by one or all of the following: (1) feeding of the 15.11-Mev level by higher levels in C^{12} , (2) the incomplete absorption by the NaI(Tl) crystal of higher energy photons scattered by the target, and (3) background produced by neutrons generated in the target. This background was determined by making a self-absorption measurement⁸ with a 2-g/cm² carbon absorber in the incident beam when the betatron was operated at energies above and below 20 Mev. At 40 Mev the background amounted to a 10% correction.

Each run was monitored in terms of the charge collected from the transmission ionization chamber. This chamber was calibrated by comparing its reading with that of a standard chamber placed in the same beam. The standard chamber had been calibrated by the total spectrum method of Koch, Leiss, and Pruitt.⁹

The properties of the various targets used are listed in Table I. The target normally used in the betatron is a tungsten wire with a diameter of 0.025 inch. This target is located at a smaller radius than the equilibrium orbit in the betatron. The other targets were mounted, four at a time, in a special holder that allowed any one of the four to be rotated into position within the donut without breaking the vacuum or changing the donut position. These targets were all positioned at a radius larger than the equilibrium orbit but inside the radius of the injector.

In the case of the normal betatron target, x-rays were obtained by applying a rather slow pulse to an electron-orbit shift coil whose radius was smaller than that of the donut. The x-ray pulse from the betatron under these conditions was roughly triangular in shape with a base length of about 4 microseconds. For the data taken near the threshold for scattering by the 15.11-Mev line, the time width of the x-ray pulse and the rate of change of the betatron magnetic field resulted in an energy

spread of about 80 kev. For the targets mounted at a radius larger than the equilibrium orbit, yield was obtained by applying a large pulse to a pair of coils located above and below the equilibrium orbit. This procedure resulted in an x-ray pulse whose width was less than 0.1 microsecond at the base. In this case the spread of the beam was less than 2 kev.

During all spectrum measurements, the x-ray intensity from the betatron was kept below a limit fixed by the counting rate of an integral discriminator biased at about 1 Mev. This limit was fixed at about one-half the counting rate at which pile-up was observed in the region *A* to *B* of the pulse-height distribution given in Fig. 2, when the yield of counts in this region was measured as a function of the counting rate of the integral discriminator. The measurements were made for both the "slow-contract" and the "fast-expand" targets.

The energy scale of the betatron was based on the thresholds for the (γ, n) reactions in Be⁹, Au¹⁹⁷, and Cu⁶⁵ and on the threshold for scattering by the 15.11-Mev level in C^{12} . The latter threshold is by far the sharpest observed in this laboratory. A change of 20 kev on the energy scale produced a fivefold increase in counting rate. The threshold for this scattering was used to monitor any changes in the betatron energy scale. As would be expected, the energy calibration was different for the "expand" target and for the "contract" target. For any one type of machine operation, however, the energy calibration was constant to within 20 kev for the three-month period during which measurements were made. It was found that this stability could be obtained by warming up the betatron for about one hour before starting to take data.

For each of the targets used an attempt was made to determine the effective target thickness by measuring the angular distribution of the bremsstrahlung. These measurements were made by exposing a copper strip on the betatron side of the collimator. The strip was located on a diameter of the beam (see Fig. 1). After exposure of the strip to either 19- or 21-Mev bremsstrahlung (the energy differed for different targets), the 10-minute activity induced in the strip was counted as a function of position across the strip. After corrections were made for the decay of the induced radioactivity, the data gave the angular distribution for those photons in the high-energy part of the bremsstrahlung spectrum. Strips were exposed both vertically and horizontally. The angular distributions were not different within the errors of measurement. The measured angular distributions were used to determine the effective target thicknesses by comparing them with the angular distribution given by Muirhead *et al.*¹⁰ For the 0.001-inch tungsten and 0.002-inch thorium targets there seems to be some evidence for multiple traversals of the target, since the target thicknesses in kev as inferred from

TABLE I. Target properties.

Target	Energy loss ^a kev	Beam width at one-half maximum Mev-radians	Observed energy loss ^b kev
0.025 in. W wire	1100	2.3	130 ± 40
0.001 in. W foil	44	2.0	117 ± 23
0.010 in. W foil	440	2.7	370 ± 70
0.010 in. Ni foil	240	2.4	350 ± 84
0.002 in. Th foil	49	2.3	112 ± 34

^a Based on collision-energy loss expression as given by Goldwasser, Mills, and Hanson, *Phys. Rev.* **88**, 1137 (1952).

^b Based on Muirhead *et al.* (reference 10) and on measured angular distribution of the bremsstrahlung beam.

⁹ Koch, Leiss, and Pruitt, *Bull. Am. Phys. Soc. Ser. II*, **1**, 199 (1956).

¹⁰ Muirhead, Spicer, and Lichtblau, *Proc. Phys. Soc. (London)* **A65**, 59 (1952).

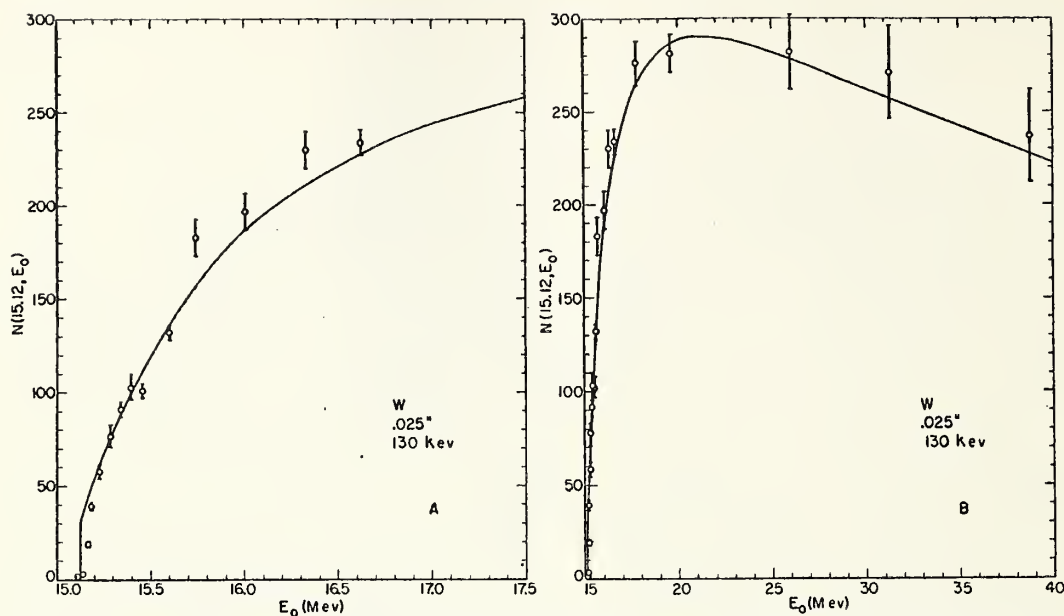


FIG. 3. The yield of 15.12-Mev photons obtained when electrons of energy, E_0 , were slowly contracted into the 0.025-inch wire target normally used in the betatron. The solid curve is the Schiff spectrum normalized to the experimental curve near 20 Mev. The target thickness, as determined by a measurement of the angular distribution of the bremsstrahlung, is 130 kev.

reference 10 were larger than the collision-energy loss expected for these foils. The data for the 0.025-inch tungsten wire target clearly show the effect of a slowly contracted beam just grazing the edge of a target.

III. RESULTS

Figure 3 shows the yield curves obtained using the 0.025-inch tungsten wire target into which the betatron electron beam was slowly contracted. The ordinates of Fig. 3 are in units of the relative number of 15.12-Mev photons per Mev in the beam. Also plotted is the yield curve obtained from the Schiff bremsstrahlung spectrum as tabulated by Penfold and Leiss.¹¹ These tables are frequently used in the analysis of activation curves. The theoretical curve has been normalized to the experimental data near 20 Mev. The approximations made by Schiff¹² in evaluating the differential bremsstrahlung cross section of Bethe and Heitler were that the energies of both the incoming and outgoing electron were large compared to the rest energy of the electron. He also neglected certain screening terms in integrating over the outgoing electron angles. In integrating over the outgoing photon angle the approximation was made that the angles involved are small. These approximations produced the finite threshold to the yield curve shown in Fig. 3(a). If the theoretical curve shown in Fig. 3(a) is modified, by a method to be described later, to take into account the finite thickness of the target and the energy spread of the primary electrons, a con-

siderably better fit can be obtained to the experimental data for energies near the threshold. The agreement of the experimental curve with the modified theoretical curve near threshold is only fortuitous, since the approximations made by Schiff are not valid in this energy region.

The yield curve for the tungsten-wire target was measured for electron energies up to 40 Mev, and is given in Fig. 3(b). The coincidence of the measured and calculated yield curves demonstrates, within the rather large experimental errors, the validity of the energy dependence of the monitor calibration used for these interpretations as well as the general validity of the Schiff calculations. The data are not accurate enough to distinguish between the Schiff integrated spectrum and the corrected forward spectrum.¹³

Figure 4 shows the measured yield curves obtained by using the "thin" targets into which the electron beam was expanded.¹⁴ The solid curves are plots of a 15.12-Mev photon calculated from the Bethe-Heitler expression⁷ normalized to the experimental data at 16.75 Mev.¹⁵ This formula represents the brems-

¹³ A. Sirlin, Phys. Rev. 106, 637 (1957); E. Hisdal, Phys. Rev. 105, 1821 (1957).

¹⁴ Data were also taken by using a 0.020-inch aluminum target. These were not considered reliable because there was evidence that the x-rays came from two sources in the betatron. The measured angular distribution was very broad and the spectrum and magnitude of the yield obtained were consistent with the assumption that the x-rays came from both the aluminum target and the tungsten support for the assembly. The aluminum target was the only one for which this effect was expected.

¹⁵ The normalization factor was a function of Z , varying by 11% from nickel to thorium. This difference is of the right magnitude and sign to be attributed to a screening effect.

¹¹ A. S. Penfold and J. E. Leiss, Phys. Rev. 95, 637 (1954); and private communication.

¹² L. I. Schiff, Phys. Rev. 83, 252 (1951).

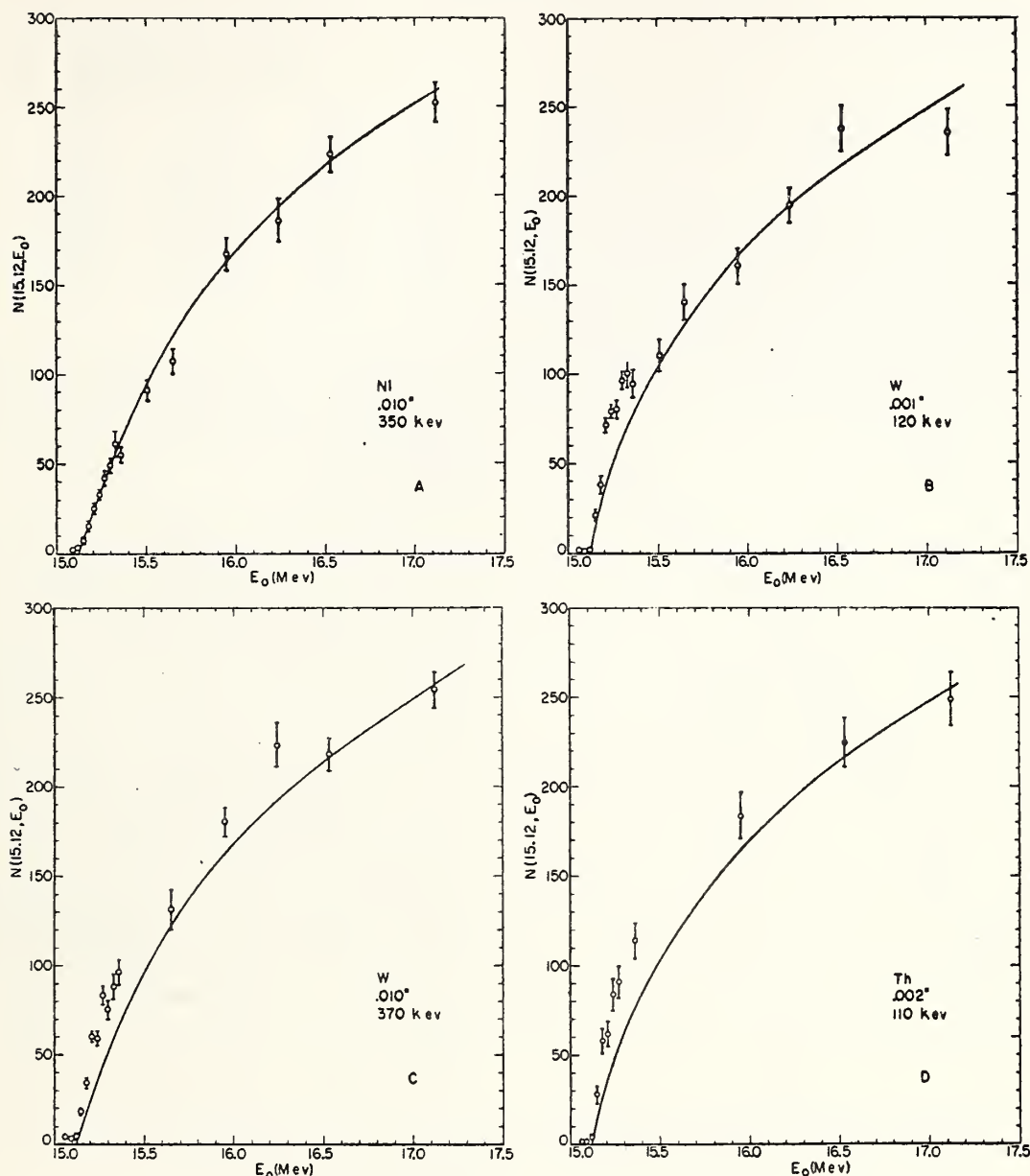


FIG. 4. The yield curves obtained when the electrons were rapidly expanded into targets of 0.010-inch nickel, 0.001-inch tungsten, 0.010-inch tungsten, and 0.002-inch thorium foils. The solid curves have been calculated from the Bethe-Heitler formula modified to take into account target thickness effects. Target thickness used was that determined from a measurement of the angular distribution of the bremsstrahlung from each target. This thickness is given in kev.

strahlung cross section integrated over the outgoing electron and photon angles. It should provide a more legitimate test of the validity of the Born approximation than would Schiff's calculation. The value of zero for the cross section at the threshold of the yield curve is a consequence of the Born approximation. It is evident that the experimental yield curves rise more rapidly from threshold for the heavier nuclei than do the theoretical curves.

The theoretical curves shown in Fig. 4 have all been

modified to take into account the finite thickness of the various targets. The target thickness used for each target is given in kev on the graphs. The effective target thicknesses were determined from the angular distribution as described above. The distortions produced by multiple scattering and energy loss in the target may be taken into account by integrating the contributions to the bremsstrahlung generated in elements of target thickness, dx .¹⁶ If $N(15,12, E_0)$ is the elementary yield

¹⁶ Motz, Miller, and Wyckoff, Phys. Rev. 89, 968 (1953).

curve, then the modified curve will be:

$$N'(15.12, E_0) = \int_0^T dx S(x) N\left(15.12, E_0 + \frac{dE}{dx}\right),$$

where $S(x)$ is the probability that a photon generated in dx is detected. $S(x)$ therefore depends on the target properties and the acceptance angle of the detector. The functions, $S(x)$, have been calculated using a procedure outlined by Penfold¹⁷ for the targets and the acceptance angle of 0.01 radian used in this experiment. In this approximation energy loss and scattering were treated as independent processes and radiation strag-

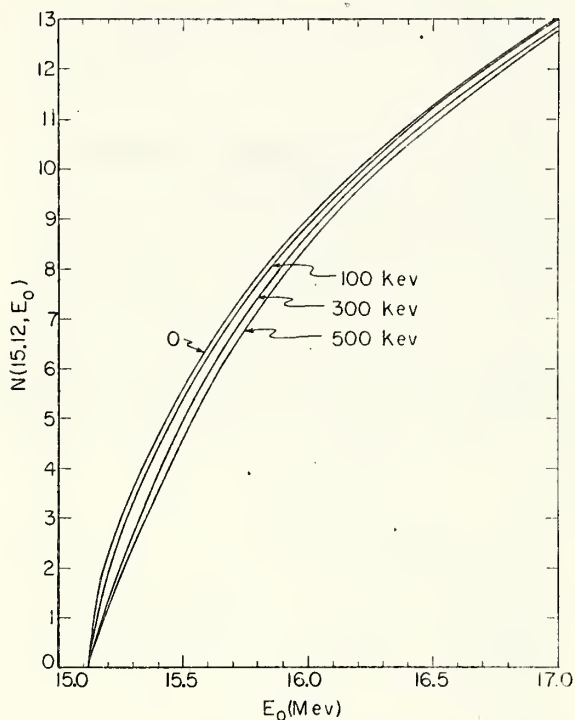


FIG. 5. A comparison of the calculated thin-target yield curve with those modified for tungsten targets 100, 300, and 500 keV thick.

gling was completely neglected. Penfold has shown that these simplifications do not alter the results significantly, but do make hand computation feasible.

The effects of the finite target thickness on the shape of a yield curve are shown in Fig. 5. The upper curve is a plot of the undistorted 15.12-Mev yield curve calcu-

¹⁷ A. S. Penfold (private communication).

TABLE II. Ratio of observed counts/Mev to the modified Bethe-Heitler distribution.

Energy	Ni 0.010 in.	W 0.001 in.	W 0.010 in.	Th 0.002 in.
15.51	0.96±0.06	1.05±0.10		
15.36	0.87±0.06	1.22±0.10	1.48±0.11	1.48±0.13
15.33	1.09±0.13	1.43±0.11	1.50±0.12	
15.30	1.02±0.08	1.52±0.08	1.50±0.10	
15.27	1.05±0.10	1.45±0.10	1.98±0.12	1.63±0.16
15.24	1.03±0.10	1.68±0.08	1.74±0.12	1.78±0.19
15.21	1.0 ±0.12	1.92±0.11	2.4 ±0.12	1.68±0.17

lated from the Bethe-Heitler formula. The three lower curves resulted from folding the thick target weighting functions, $S(x)$, into the latter to take into account the effects of energy loss and multiple scattering in tungsten targets 100, 300, and 500 keV thick. The differences are not very great.

A cursory inspection of Fig. 4 reveals that the yield curve measured using the nickel target agrees well with that given by the Bethe-Heitler formula corrected for target thickness. Within 300 keV of the tip of the spectrum the tungsten and thorium data lie above the calculated distributions. The ratio of the experimental points of Fig. 4 to the modified Bethe-Heitler distribution in the energy range 15.12 to 15.51 Mev are given in Table II. The ratios of the order of two near the tip for high atomic number targets are similar in magnitude to those found by Starfelt and Koch¹ for very thin gold targets and similar outgoing electron energies. These data indicate that for the heavy target nuclei there is an excess in the number of photons in the high-energy tip of the bremsstrahlung spectrum over that given by the Born-approximation calculation. The data may also indicate that there is a finite value for the end of the bremsstrahlung spectrum which depends somewhat upon the nuclear charge. To be consistent with the present data, this end point cannot vary faster than $Z^{\frac{1}{2}}$. An exact calculation is expected to result in a finite end point to the spectrum.¹⁸ None of the various attempts to approximate a correction to the Bethe-Heitler cross section yields a result consistent with the data given in Table II.

ACKNOWLEDGMENT

The authors wish to thank Irwin Oppenheim for his interest and Ida Reingold for her help in the evaluations of the Bethe-Heitler cross section.

¹⁸ F. G. Nagasaka, Ph.D. thesis, University of Notre Dame, 1955 (unpublished); E. Guth, Phys. Rev. **59**, 325 (1941); G. Elwert, Ann. Physik **34**, 178 (1939).



DISTRIBUTION LIST

GOVERNMENTAL

<u>No. of Copies</u>	<u>Agency</u>
5	Commander Air Force Office of Scientific Research Air Research and Development Command ATTN: SRY Washington 25, D C
4	Commander Wright Air Development Center ATTN: WCOSI-3 Wright-Patterson Air Force Base, Ohio
1	Commander Air Force Cambridge Research Center ATTN: Technical Library L. G. Hanscom Field Bedford, Mass.
1	Commander Rome Air Development Center ATTN: RCSST-4 Rome, New York
1	Director, Office for Advanced Studies Air Force Office of Scientific Research Air Research & Development Command Post Office Box 2035 Pasadena 2, California
2	Commander European Office Air Research & Development Command 47 rue Cantersteen Brussels, Belgium (Air Mail)
10	Commander ASTIA ATTN: TIPDR Arlington Hall Station Arlington 12, Virginia
1	Director of Research & Development Headquarters USAF ATTN: AFDRD Washington 25, D. C.

Distribution List (Continued)

<u>No. of Copies</u>	<u>Agency</u>
1	Chief of Naval Research Department of the Navy ATTN: Code 420 Washington 25, D. C.
1	Director, Naval Research Laboratory ATTN: Technical Information Officer Washington 25, D. C.
1	Director, Research & Development Division General Staff Department of the Army Washington 25, D. C.
1	Chief, Physics Branch, Division of Research U. S. Atomic Energy Commission Washington 25, D. C.
1	U. S. Atomic Energy Commission Technical Information Extension Post Office Box 62 Oak Ridge, Tenn.
1	National Bureau of Standards Library Room 301, Northwest Building Washington 25, D. C.
1	National Science Foundation 1520 H Street, N. W. Washington 25, D. C.
1	Director, Office of Ordnance Research Box CM, Duke Station Durham, North Carolina
1	Office of Technical Services Department of Commerce Washington 25, D. C.
1	Commander Arnold Engineering Development Center ATTN: Technical Library Tullohoma, Tenn.
1	Commander Air Force Armament Center ATTN: Technical Library Eglin Air Force Base, Florida

Distribution List (Continued)

<u>No. of Copies</u>	<u>Agency</u>
1	Commander Air Force Flight Test Center ATTN: Technical Library Edwards Air Force Base, Calif.
1	Commander Air Force Missile Test Center ATTN: Technical Library Patrick Air Force Base Cocoa, Florida
1	Commander Air Force Speical Weapons Center ATTN: Technical Library Kirtland Air Force Base, New Mexico
1	Commander Air Force Missile Development Center ATTN: Technical Library Holloman Air Force Base, New Mexico
1	Commander AF Cambridge Research Center ATTN: CROOIR L. G. Hanscom Field Bedford, Mass.
1	Commander Army Rocket & Guided Missile Agency Redstone Arsenal ATTN: ORDXR-OTL Alabama
1	Commandant Air Force Institute of Technology ATTN: MCLI, Technical Library Wright-Patterson Air Force Base, Ohio
1	Commander Air Force Ballistic Missile Division Headquarters ARDC ATTN: WDSOT Post Office Box 262 Inglewood, Calif.
1	

Distribution Lis (Continued)

No. of Copies

Agency

1

Applied Mechanics Reviews
Southwest Research Institute
8500 Culebra Road
San Antonio 6, Texas

1

Institute of the Aeronautical Sciences
ATTN: Librarian
2 East 54th Street
New York 16, New York

U. S. DEPARTMENT OF COMMERCE

Lewis L. Strauss, *Secretary*

NATIONAL BUREAU OF STANDARDS

A. V. Astin, *Director*



THE NATIONAL BUREAU OF STANDARDS

The scope of activities of the National Bureau of Standards at its headquarters in Washington, D. C., and its major laboratories in Boulder, Colo., is suggested in the following listing of the divisions and sections engaged in technical work. In general, each section carries out specialized research, development, and engineering in the field indicated by its title. A brief description of the activities, and of the resultant publications, appears on the inside front cover.

WASHINGTON, D. C.

Electricity and Electronics. Resistance and Reactance. Electron Devices. Electrical Instruments. Magnetic Measurements. Dielectrics. Engineering Electronics. Electronic Instrumentation. Electrochemistry.

Optics and Metrology. Photometry and Colorimetry. Optical Instruments. Photographic Technology. Length. Engineering Metrology.

Heat. Temperature Physics. Thermodynamics. Cryogenic Physics. Rheology. Engine Fuels. Free Radicals Research.

Atomic and Radiation Physics. Spectroscopy. Radiometry. Mass Spectrometry. Solid State Physics. Electron Physics. Atomic Physics. Neutron Physics. Radiation Theory. Radioactivity. X-rays. High Energy Radiation. Nucleonic Instrumentation. Radiological Equipment.

Chemistry. Organic Coatings. Surface Chemistry. Organic Chemistry. Analytical Chemistry. Inorganic Chemistry. Electrodeposition. Molecular Structure and Properties of Gases. Physical Chemistry. Thermochemistry. Spectrochemistry. Pure Substances.

Mechanics. Sound. Mechanical Instruments. Fluid Mechanics. Engineering Mechanics. Mass and Scale. Capacity, Density, and Fluid Meters. Combustion Controls.

Organic and Fibrous Materials. Rubber. Textiles. Paper. Leather. Testing and Specifications. Polymer Structure. Plastics. Dental Research.

Metallurgy. Thermal Metallurgy. Chemical Metallurgy. Mechanical Metallurgy. Corrosion. Metal Physics.

Mineral Products. Engineering Ceramics. Glass. Refractories. Enameled Metals. Concreting Materials. Constitution and Microstructure.

Building Technology. Structural Engineering. Fire Protection. Air Conditioning, Heating, and Refrigeration. Floor, Roof, and Wall Coverings. Codes and Safety Standards. Heat Transfer.

Applied Mathematics. Numerical Analysis. Computation. Statistical Engineering. Mathematical Physics.

Data Processing Systems. SEAC Engineering Group. Components and Techniques. Digital Circuitry. Digital Systems. Analog Systems. Application Engineering.

- Office of Basic Instrumentation.
- Office of Weights and Measures.

BOULDER, COLORADO

Cryogenic Engineering. Cryogenic Equipment. Cryogenic Processes. Properties of Materials. Gas Liquefaction.

Radio Propagation Physics. Upper Atmosphere Research. Ionospheric Research. Regular Propagation Services. Sun-Earth Relationships. VHF Research. Ionospheric Communication Systems.

Radio Propagation Engineering. Data Reduction Instrumentation. Modulation Systems. Navigation Systems. Radio Noise. Tropospheric Measurements. Tropospheric Analysis. Radio Systems Application Engineering. Radio-Meteorology.

Radio Standards. High Frequency Electrical Standards. Radio Broadcast Service. High Frequency Impedance Standards. Electronic Calibration Center. Microwave Physics. Microwave Circuit Standards.

